Property Changes of Deep and Bottom Waters in the Western Tropical Atlantic

Josefine Herrford, Peter Brandt, Walter Zenk

PII: S0967-0637(16)30049-8
DOI: http://dx.doi.org/10.1016/j.dsr.2017.04.007
Reference: DSRI2778

To appear in: *Deep-Sea Research Part I*

Received date: 9 February 2016
Revised date: 6 April 2017
Accepted date: 7 April 2017

Cite this article as: Josefine Herrford, Peter Brandt and Walter Zenk, Property Changes of Deep and Bottom Waters in the Western Tropical Atlantic, *Deep-Sea Research Part I,* http://dx.doi.org/10.1016/j.dsr.2017.04.007

Property Changes of Deep and Bottom Waters in the Western Tropical Atlantic

Josefine Herrford*, Peter Brandt, Walter Zenk

GEOMAR Helmholtz Centre for Ocean Research Kiel, Düsternbrooker Weg 20, 24105 Kiel, Germany

jherrford@geomar.de (J. Herrford) *

pbrandt@geomar.de (P. Brandt)

wzenk@geomar.de (W. Zenk)

* Corresponding author

Abstract

The flow of North Atlantic Deep Water (NADW) and Antarctic Bottom Water (AABW) contributes to the Atlantic meridional overturning circulation. Changes in the associated water mass formation might impact the deep ocean's capacity to take up anthropogenic CO_2 while a warming of the deep ocean significantly contributes to global sea level rise. Here we compile historic and recent shipboard measurements of hydrography and velocity to provide a comprehensive view of water mass distribution, pathways, along-path transformation and long-term temperature changes of NADW and AABW in the western South and Equatorial Atlantic. We confirm previous results which show that the northwest corner of the Brazil Basin represents a splitting point for the southward/northward flow of NADW/AABW. The available measurements sample water mass transformation along the two major routes for deep and bottom waters in the tropical to South Atlantic – along the deep western boundary and eastward, parallel to the equator - as well as the hot-spots of extensive mixing. We find lower NADW and lighter AABW to form a highly interactive transition layer in the northern Brazil Basin. The AABW north of 5°S is relatively homogeneous with only lighter AABW being able to pass through the Equatorial Channel (EQCH) into the North Atlantic. Spanning a period of 26 years, our data also allow an estimation of long-term temperature trends in abyssal waters. We find a warming of $2.5 \pm 0.7 \cdot 10^{-3}$ °C yr^{-1} of the waters in the northern Brazil Basin at temperatures colder than 0.6 °C throughout the period 1989-2014 and can relate

this warming to a thinning of the dense AABW layer. Whereas isopycnal heave is the dominant effect which defines the vertical distribution of temperature trends on isobars, we also find temperature changes on isopycnals in the lower NADW and AABW layers. There temperatures on isopycnals exhibit decadal variations with warming in the 1990s and cooling in the 2000s - the contributions to the trends on isobars range from about 50% in the lighter AABW layers in the EQCH up to a maximum of 80% in the transition layer the lower NADW and lighter AABW form in the northern Brazil Basin.

Keywords*:* Northern Brazil Basin, Antarctic Bottom Water, North Atlantic Deep Water, abyssal circulation, AABW warming

1. INTRODUCTION

The meridional overturning circulation of the tropical and subtropical South Atlantic (AMOC) consists essentially of three meridional flows that separate two cells: The upper cell is formed by the northward flowing warm waters near the surface and the southward flowing cold waters at deeper levels, the North Atlantic Deep Water (NADW; see a list of abbreviations in Table 1), and the lower cell is formed by the same southward flowing NADW and the northward flowing Antarctic Bottom Water (AABW) just above the sea floor (Lumpkin and Speer, 2007). In a global context, both overturning cells are of about the same strength, although the deeper one is of smaller vertical extend and carries less heat in the Atlantic Ocean (Orsi et al., 1999). The western equatorial Atlantic is a highly active crossroad for the different branches of these overturning cells and thus represents a key region for the interhemispheric water exchange. Our study focuses on the spatial and temporal property changes of NADW and AABW in the western tropical Atlantic (37°W-19°W/15°S-10°N).

a) Hydrography

In the western boundary regime of the tropical Atlantic, the NADW typically occupies a layer between 1200 – 4000 m (e.g. Schott et al., 2003) characterized by higher salinity, temperature and oxygen concentrations than the surrounding waters (Wüst, 1935; Larque et al., 1997; Vanicek and Siedler, 2002). The literature typically separates the NADW into at least three parts of different origin: The densest water component of the NADW is commonly referred to as Denmark Strait Overflow Water (DSOW) at higher latitudes, or as “lower NADW (lNADW)” farther south. Middle NADW (mNADW) originates from water overflowing the sills east of Iceland (Iceland-Scotland Overflow Water (ISOW); Dickson and Brown, 1994) which is modified by entrainment of ambient waters on its way through the Iceland Basin,

gaps in the Mid-Atlantic Ridge (MAR), and the Irminger Basin. In the North Atlantic, the DSOW can be identified by a deep oxygen maximum with ISOW having comparatively reduced oxygen levels in the western basin (e.g., Mantyla and Reid, 1983; van Aken and de Boer, 1995). As they progress along the continental slopes of Greenland and Eastern Canada, both water masses are joined by a lighter water mass, namely the Labrador Sea Water (LSW), which is formed by deep wintertime convection in the Labrador and Irminger Seas (e.g., Pickart et al., 2003; Kieke and Yashayaev, 2015). Often referred to as the upper NADW (uNADW), the LSW is characterized by high oxygen content due to its recent exposure to the atmosphere (Pickart et al., 2003). It should be noted that several studies in the tropical and South Atlantic distinguish a fourth component, as a pronounced salinity maximum is observed just above the oxygen maximum of the LSW - believed by some to be a different vintage of LSW (e.g., Rhein et al., 1995; 1998; Vanicek and Siedler, 2002) while others discuss a contribution of Mediterranean Sea Water (e.g., Arhan et al., 1998). In the northern Brazil Basin, older modified or recirculated water masses from the western boundary, eastern Atlantic or southern Brazil Basin join the southward flow of NADW off Brazil, thereby diluting the water masses of northern origin (e.g. Friedrichs et al., 1994). Furthermore it has been shown for the tropical Atlantic that the distinction between the different source water masses of NADW becomes more difficult. South of 20°S, according to Demidov (2003), the division of NADW into components "is not justified anymore due to the absence of mNADW and strong similarity between uNADW and lNADW". Nevertheless, the relatively warm, salty and oxygen-rich signature of the remaining NADW is known to reach the latitudes of the Antarctic Circumpolar Current (ACC) where it is referred to as part of the Circumpolar Deep Water (CDW; Peterson and Whitworth III, 1989).

The coldest bottom waters of Antarctic origin are often collectively referred to as Antarctic Bottom Water. According to the concept of Orsi et al. (1999), a variety of noticeably dense bottom waters is formed over the Antarctic shelf. This process involves source water cooling due to heat loss and salinity increase due to sea ice formation and brine rejection, in addition to mixing of the cold and dense Antarctic Shelf Waters with warmer, more saline old deep waters such as the CDW. In the South Atlantic Ocean, several studies support the division of AABW into two components: The denser component with potential temperatures (θ) below 0 – 0.2 °C is typically a modified version of Weddell Sea Deep Water (WSDW) spreading into the Argentine Basin (Reid et al., 1977). Mantyla and Reid (1983), Tsuchiya et al. (1994) or Sandoval and Weatherly, (2001) stated that the lighter component is rather Lower Circumpolar Water (LCPW [1]), which is characterized by potential temperatures (θ) below 2 °C and low oxygen concentrations. Following Orsi et al. (1999), LCPW is exported from the deep levels of the ACC

[1] According to Tarakanov (2012) the widely used term LCPW needs to be applied with care. He suggests the names ACC Bottom Water (ACCbw; following Orsi et al., 1999), Circumpolar Bottom Water (CBW) or Antarctic Deep Water (AADW) for this component.

covering the layer between the denser southern bottom water below and the salinity maximum of the CDW above. In the Brazil Basin, LCPW is thought to make up the larger portion of AABW (e.g., Speer and Zenk, 1993), while north of 10°S many authors notice a disappearance of the WSDW (e.g., Reid, 1989; Sandoval and Weatherly, 2001), which in turn leaves only the LCPW to reach the equator. On its way north, the cold and fresh AABW encounters the lighter overlying NADW, with both water masses creating an abyssal stratification and gradual mixing along their interface. This is associated with more abrupt property changes at sills, in narrow passages or above rough bottom topography where mixing is typically enhanced (e.g., Polzin et al., 1997). Upon its arrival in the equatorial Atlantic, the AABW has become much warmer, saltier and oxygenated, with almost linearly decreasing temperature and salinity profiles towards the bottom (Rhein et al., 1998).

Table 1 List of abbreviations.

AABW	Antarctic Bottom Water
AADW	Antarctic Deep Water
ACCbw	ACC Bottom Water
AAIW	Antarctic Intermediate Water
ACC	Antarctic Circumpolar Current
CDW	Circumpolar Deep Water
CFM	Chlorofluoromethane
CTD	Conductivity-Temperature-Depth
DSOW	Denmark Strait Overflow Water
DWBC	Deep Western Boundary Current
EQCH	Equatorial Channel
HCH	Hunter Channel
ISOW	Iceland Scotland Overflow Water
LADCP	Lowered Acoustic Doppler Current Profiler
LCPW	Lower Circumpolar Water
LSW	Labrador Sea Water
MAR	Mid-Atlantic Ridge
(A)MOC	(Atlantic) Meridional Overturning Circulation
NADW	North Atlantic Deep Water
RCHFZ	Romanche and Chain Fracture Zones
SACW	South Atlantic Central Water
VCH	Vema Channel
WDW	Warm Deep Water
WOCE	World Ocean Circulation Experiment
WSBW	Weddell Sea Bottom Water
WSDW	Weddell Sea Deep Water

b) Pathways

Originating from the subpolar North Atlantic, NADW is known to enter the subtropics as part of the Deep Western Boundary Current (DWBC), which spreads southward in the western Atlantic basin (Figure 1a). Aside from the DWBC, there exist recirculation cells to the East (e.g., McCartney, 1992) and other interior routes (e.g., Bower et al., 2009). In the tropical Atlantic, transport of the DWBC was estimated to be 17 – 25 Sv (1 Sv = 10^6 m^3 s^{-1}) flowing towards and across the equator (e.g., Hall et al., 1997; Rhein et al., 1995, 1998). Additionally, an elongated cyclonic recirculation gyre was observed in the Guiana Basin (e.g., Friedrichs et al., 1994; Wienders et al., 2000; Sarafanov et al., 2007). At 35°W, the deep Equatorial Channel (EQCH) was found to guide the flow of NADW eastward. While the denser NADW components were encountered as a focused velocity core just north of the Parnaiba Ridge (Rhein et al., 1995), the uNADW also flows closer to the coast as a contour-following current along the topography of the continental margin (Schott et al., 2003). Crossing the equator, the NADW immediately bifurcates – into an eastward flow parallel to the equator and a southward flow continuing along the western slope as the DWBC. The eastward pathway was first proposed by Weiss et al. (1985) and subsequently documented by Mercier and Morin (1997) and Messias et al. (1999) by tracing the NADW through the Romanche and Chain Fracture Zones (RCHFZ). Tracking neutrally buoyant floats at a depth of 1800 m, Richardson and Fratantoni (1999) inferred the eastward jets of the equatorial current system to be directly fed by waters of the DWBC and found indications for a return flow from the MAR back into the DWBC region via slow interior pathways. At 23°W, Gouriou et al. (2001) found an eastward velocity core at about 3800 m and l.5°S related to the lNADW layers at 35°W. The presence of nearly barotropic eastward jets parallel to the equator at about 2°N and 2°S, which were later also found in an ensemble average of several 23°W sections (Greatbatch et al., 2012), was theoretically suggested to be the result of rectification of deep equatorial intra-seasonal variability (Ascani et al., 2010; 2015). Studying the flow along the western boundary, Friedrichs et al. (1994) suggested a hemispheric contrast in the dominant transport mode: In addition to a strong DWBC transport of lNADW with an associated recirculation in the Guiana Basin and a narrow eastward flow parallel to the equator, they also observed a broader opposing flow of mNADW from the East towards the western boundary. This flow then bifurcates to supply the southward DWBC as well as the northward flow of mNADW in the Guiana Basin recirculation gyre. The southward branch of mNADW reinforces and dominates the DWBC in the South Atlantic and, turning northeastward just north of the Vitória-Trindade Ridge, forms a second abyssal recirculation gyre in the northern Brazil Basin (cf. Figure 1a). The required water mass transformation from lNADW into lighter density classes was found to be in general agreement with an inverse study of Lux et al. (2001) and an observational study of Schott et al. (2005). Using shipboard and moored observations, Schott et al. (2005) reported a drastic decrease of the lNADW transport – from 7 Sv eastward at 35°W compared to 1.5 Sv southward in the DWBC at 5°S.

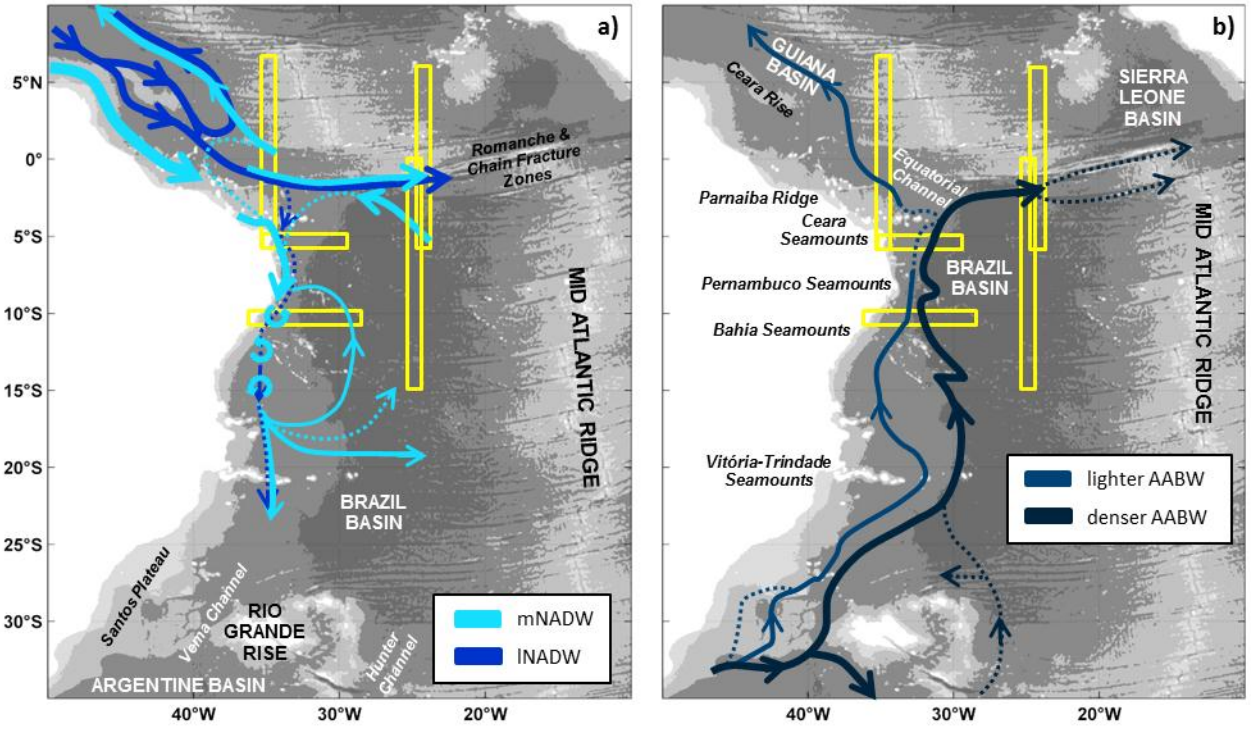

Figure 1 Bathymetric charts of the South and Tropical Atlantic Ocean (with contour intervals of 1000 m) including all relevant topographic features. Yellow boxes indicate the location of repeated ship sections. Dashed lines show uncertain pathways. a) Schematic of assumed pathways of mNADW and lNADW, modified from Friedrichs et al. (1994) and following the ideas of Arhan et al. (1998), Dengler et al. (2004), Garzoli et al. (2015). b) Schematic of assumed pathways of lighter and denser AABW components, modified from Morozov et al. (2010, p.184), following the ideas of Larque et al. (1997), Sandoval and Weatherly (2001) and Tarakanov and Morozov (2015).

Farther south at 11°S, Dengler et al. (2004) showed that the NADW transport "is accomplished by migrating eddies, rather than by a continuous flow." This eddy-dominated flow continues southward to the Vitória-Trindade Ridge where preservation of potential vorticity results in a branching of the flow. The DWBC was found to split into one or even several zonal current branches between 19°S and 30°S, with about 20% of the water flowing eastward into the interior South Atlantic (e.g., Hogg and Owens, 1999; Vanicek and Siedler, 2002; Hogg and Thurnherr, 2005; Garzoli et al., 2015).

South of 30°S, the flow of NADW is mainly oriented southwards again (e.g., Larque et al., 1997; Meinen et al., 2012; Garzoli et al., 2015). The remaining NADW reaches the latitudes of the ACC where it is then deflected eastward around the Antarctic continent (e.g.; Mantyla and Reid, 1983).

The flow and distribution of Antarctic waters in the bottom layer of the Atlantic Ocean is strongly guided by bottom topography. Many years after their formation, the LCPW and different vintages of WSDW arrive at the Rio Grande Rise where both water masses can exit the Argentine Basin to the North as AABW. The flow of AABW mainly occurs through the Vema and Hunter channels (VCH and HCH) - transports through the VCH and HCH were estimated to be 4 Sv and 3 Sv, respectively (Hogg et al.,

1999; Zenk et al., 1999) - but also extends over deeper parts of the Santos Plateau (e.g., Sandoval and Weatherly, 2001). There is much discussion in the literature as to which fractions of the WSDW and LCPW pass through the channels and how variable these flows are (e.g., Speer and Zenk, 1993; Larque et al., 1997; Zenk and Visbeck, 2013; Taraknov and Morozov, 2015). Most studies agree that, at least in part, the AABW propagates along the western slope northward to approximately 5°S (Figure 1b). Sandoval and Weatherly (2001) presented a circulation scheme in which two almost parallel main flows can be traced from VCH to about 16°S and then turn together around the Vitória-Trindade seamount chain. In their opinion, the more interior flow propagates around the Bahia Seamount to then turn eastward near 4°S to the RCHFZ, while the shallower flow continues along the western boundary towards the equator. In contrast, Hogg and Owens (1999) described an interior AABW flow that is predominantly zonal rather than meridional. In the equatorial Atlantic, the AABW leaves the Brazil Basin along two routes: One route is through the RCHFZ into the East Atlantic - Mercier and Speer (1998) derived a joint transport of 1.22 ± 0.25 Sv, and Demidov et al. (2007) found 0.15 – 0.78 Sv. The other route of AABW exits the Brazil Basin through the EQCH from where it flows into the Guiana Basin. This westward flow is found to be rather confined to the southern half of the channel (e.g., Rhein et al., 1995), with transport estimates ranging from 1 – 4 Sv (e.g., Hall et al., 1997; Rhein et al., 1995, 1998; Schott et al., 2003; Limeburner et al., 2005). In the western North Atlantic, remnants of AABW continue flowing north into the North American Basin (at 24.5°N; Johnson et al., 2008; Frajka-Williams et al., 2011) and may even reach the southeastern rise of the Grand Banks of Newfoundland (e.g., McCartney, 1992).

c) AABW warming

Recent observations show a warming of the AABW during the last decades in the western South Atlantic (e.g., Johnson and Doney, 2006; Johnson et al., 2014), in the eastern Indian Ocean and throughout the Pacific (e.g., Fukasawa et al., 2004; Johnson et al., 2008; Purkey and Johnson, 2010). This AABW warming is a prominent signal of change in the global climate and can be traced by observations along the Atlantic spreading path of AABW from around Antarctica into the North Atlantic. Closest to its source region, in the Weddell Gyre, the local major water masses – Warm Deep Water (WDW[2]), WSDW and Weddell Sea Bottom Water (WSBW) – have all exhibited warming tends between the 1980s and 2000s (Robertson et al., 2002; Purkey and Johnson, 2010; Purkey and Johnson, 2013). More recently, the WDW has fluctuated between warming and cooling (Fahrbach et al., 2004; 2011). The abyssal waters in the Scotia Sea and Argentine Basin, which are both directly fed by the deep waters from the Weddell Sea, have warmed over at least the last three decades (Johnson and Doney, 2006; Purkey and Johnson, 2012).

[2] WDW is CDW that enters the Weddell Sea from the northeast and circulates at intermediate depths. It is the main source water for WSDW and WSBW (Fahrbach et al., 2011).

In the northwest corner of the Argentine Basin, Coles et al. (1996) also reported a decrease in the volume of bottom water when comparing hydrographic data from 1988 – 1989 with data collected mostly about 8 – 10 years earlier. In the VCH, Zenk and Morozov (2007) and Zenk and Visbeck (2013) found a systematic increase of the lowest bottom temperatures from repeatedly measured stations. Their evolution shows a stagnant period over 20 years until 1990, followed by significant long-term temperature increase of $2 – 3 \cdot 10^{-3}$ °C yr^{-1} until 2010.

Within the Brazil Basin, Johnson and Doney (2006) found a statistically significant (at 95% confidence limits) warming of about $2.4 – 4.4 \cdot 10^{-3}$ °C yr^{-1} on isobars between 1989/1995 and 2005/2003 in the most homogenous abyssal waters below 4500 dbar. Johnson et al. (2014) reported a similar warming trend of up to $2 – 3 \cdot 10^{-3}$ °C yr^{-1} from 1989 to 2014 at pressures greater than 4300 dbar. This result is also statistically significant and accompanied by the descending of isotherms with $\theta < 0.25$ °C up to 110 m $decade^{-1}$. At the same time they found warmer waters of $0.25 < \theta < 1.2$ °C to expand with isotherms ascending at a maximum rate of 15 m $decade^{-1}$. Analyzing hydrographic measurements in the EQCH along 35°W, Andrie et al. (2003) reported temperature at the greatest sampled pressures rising from 0.55 °C in 1993 to 0.65 °C in 1999 ($\sim 1.7 \cdot 10^{-3}$ °C yr^{-1}). Such trend was confirmed by Limeburner et al. (2005), showing water colder than 0.6 °C being present in the EQCH along 36°W about 100 m above the bottom in 1992, almost absent in 1994 and completely gone in 1999, 2001, 2003. At 7.5°N, Sarafanov et al. (2007) found a warming of $3 \cdot 10^{-3}$ °C yr^{-1} vertically averaged over the AABW layer comparing the years 1957, 1993, 2000. Farther north, Johnson et al. (2008) also used hydrographic sections to infer warming of the AABW over the last decades and a decreasing northward transport of AABW along 24.5°N from 1981 to 2004. With a more recent hydrographic section along 24°N in 2010 and measurements from a deployed mooring array there, Frajka-Williams et al. (2011) supported the AABW warming at that latitude, but estimated a partial recovery of its northward transport. The causes for the AABW warming signal in the western South Atlantic, eastern Indian Ocean and throughout the Pacific are still under investigation. Competing theories consider a reduction of AABW formation (e.g., Johnson et al., 2008; Purkey and Johnson, 2012) or a potential thermal recovery subsequent to the Weddell Polynya closing in the 1970s (Robertson et al., 2002), shifts in the formation regions of AABW around Antarctica (Shimada et al., 2012), changes in the entrainment of surrounding water masses in the AABW layer (e.g., Couldrey et al., 2013), a general shift of AABW towards lighter density classes (e.g., Azaneu et al., 2013; van Wijk and Rintoul, 2014) and restricted export from the Weddell Gyre because of strengthening westerly winds (e.g., Fahrbach et al., 2011).

The western tropical Atlantic represents a highly congested crossroad for the different branches of the AMOC. Two decades of data from an intensive observational period are available spanning the entire region. With such a unique data set it is possible to bring together different aspects of abyssal water mass

characteristics and the complex abyssal circulation. We provide a detailed study on the mean hydrography and pathways, water mass transformation and long-term temperature changes of deep and bottom waters in the northern Brazil Basin. The article is structured as follows: Chapter 2 describes the dataset used in this study. The local mean hydrography is discussed together with justifying our choice of water mass definitions in chapter 3. In chapter 4 an isopycnal view of abyssal water properties is examined and spatial changes in the θ-S-characteristics along major routes are investigated. Long-term temperature changes in the deep and bottom waters are investigated with different approaches in chapter 5. The last chapter summarizes the major results and conclusions.

2. DATA AND METHODS

2.1 Observational data

This study is based on hydrographic data and direct velocity measurements from ship sections conducted within the region 37°W-19°W/15°S-10°N, spanning the period 1989 – 2014 and going to full depth to cover abyssal waters. Its focus is on five repeated sections: Three meridional sections, all of which cross the MAR, capture the EQCH along 35°W, and cover the deep parts of the northern Brazil Basin along 25°W and the entrances to the RCHFZs along 23°W. Two zonal sections along 5°S and 11°S are used to study the southward DWBC, the northward path of the AABW below, and associated deep water recirculation cells farther east. A total of 51 hydrographic sections cover the five mean sections – 35°W (12), 25°W (7), 23°W (6), 5°S (13) and 11°S (8) – see Figure 2 and Table 2 for data availability and coverage. For a more comprehensive picture, this dataset is extended by several other ship sections occupied in this region and period once or twice (along 10°S, 36°W, 31°W, 28°W, 19°W), many of which were taken as part of the World Ocean Circulation Experiment (WOCE). The location of all measurements used here is shown in Figure 2f. Hydrographic measurements in the Vema Channel over the period 1990 – 2010 (cf. Zenk and Visbeck (2013) for a more detailed description of that dataset) are included in the analysis to represent the southern gateway into the Brazil Basin.

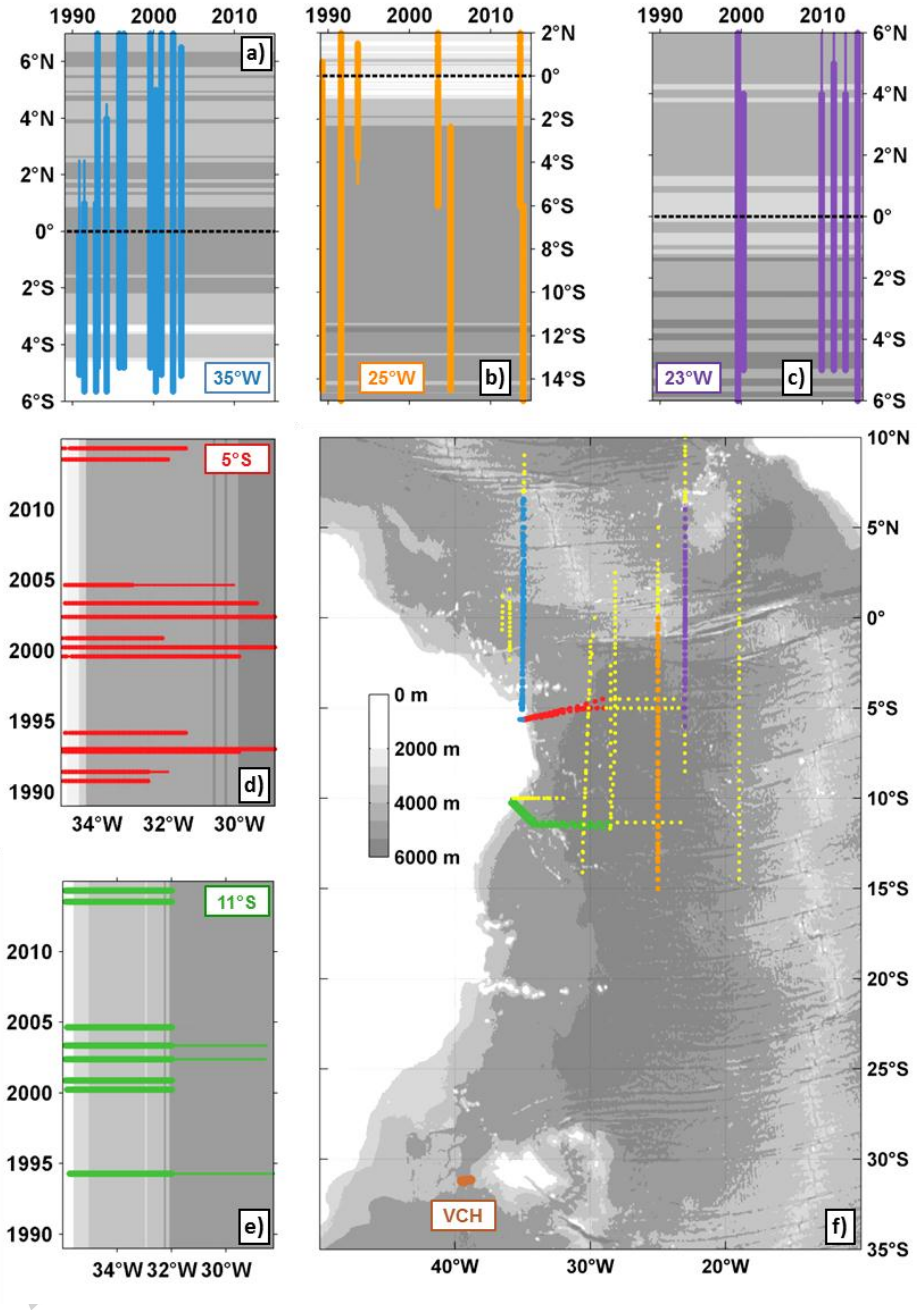

Figure 2 a-e) Temporal coverage of CTD data along each of the five repeated CTD sections. Linewidth indicates whether the profiles went to full depth (bold) or partial depth only (thin). Grey shading represents ETOPO1 bathymetry. f) Bathymetric chart of the South and Tropical Atlantic Ocean, showing the location of the ship sections analyzed in this study. Blue, orange, purple, red, green and brown dots indicate measurements of the repeated ship sections along 35°W, 25°W, 23°W, 5°S, and 11°S and across the Vema Channel. Yellow dots mark sections or segments thereof used as supplements.

Table 2 Information on availability and usage of different measurements from the ship surveys. The first column gives vessel and cruise, as well as the year (and month) for when it took place. Column 2 gives the official expocodes, an alphanumeric identifier defined by the National Oceanographic Data Center (NODC). Columns 4-6 list if CTD, O_2 or LADCP (or Pegasus) measurements are available for each of the sections, respectively, and give

the numbers of the used profiles. Colum 7 lists the data sources (** Last access: 24/11/2016). Colored backgrounds mark the data of the five repeated sections used primarily, white backgrounds mark sections or section parts used as supplement. Temperature and salinity data from "Meteor 53/2" (*) cruise in 2002 are excluded from all calculations of property changes because calibration of the CTD could not be performed with the required accuracy.

Vessel and cruise (date)	Expocode	Latitude/Longitude	Available measurements (# Profiles used)			Data source
			CTD	O_2	LADCP	
Melville HYDROS4 (Mar-Apr 1989)	318M19890313	1°S-1°N/36.5°W	6	6	-	https://cchdo.ucsd.edu/cruise/318MHYDROS4**
Knorr 142/3 (Apr-May 1994)	316N19940403	2.5°S-1.75°N/36°W	15	15	-	https://cchdo.ucsd.edu/cruise/316N142_3**
Meteor 14/2 (Oct 1990)	06M319901001	6°S-2.5°N/35°W	23	23	20 (Pegasus + LADCP)	doi:10.1594/PANGAEA.290710 | 873333 | 873335
Meteor 16/3 (May-Jun 1991)	06M319910523	6°S-2.5°N/35°W	25	25	28 (Pegasus + LADCP)	doi:10.1594/PANGAEA.290711 | 873271 | 873388
Meteor 22/2 (Oct-Nov 1992)	06M319921023	6°S-4°N/35°W	21	21	8 (only Pegasus)	doi:10.1594/PANGAEA.290713 | 873389
L'Atalante CITHER1 (Feb 1993)	35A319930102	6°S-7.5°N/35°W	28	28	-	https://cchdo.ucsd.edu/cruise/35A3CITHER1_1**
Meteor 27/3 (Feb-Mar 1994)	06M319940206	6°S-5°N/35°W	25	25	25	doi:10.1594/PANGAEA. 290714 | 319330
Le Noroit ETAMBOT1 (Sep-Oct 1995)	35LL19950909	6°S-8°N/35°W	26	26	-	https://cchdo.ucsd.edu/cruise/29HE20130320**
Edwin Link ETAMBOT2 (Apr-May 1996)	33LK19960410	6°S-8°N/35°W	26	-	28	https://cchdo.ucsd.edu/cruise/33LKETAMBOT2_1
Thalassa EQUALANT99 (Sep-Oct 1999)	35TH19990712	6°S-7°N/35°W	44	44	35	https://cchdo.ucsd.edu/cruise/35THEQUALANT9907
Meteor 47/1 (Mar-Apr 2000)	06M320000316	6°S-5°N/35°W	34	34	32	doi:10.1594/PANGAEA.787872 | 873266
Sonne 152 (Nov-Dec 2000)	06BE20001129	6°S-8°N/35°W	40	40	39	doi:10.1594/PANGAEA.742994 | 873261

Meteor 53/2 (Jan-Feb 2002)	06M32002 0506	6°S-8°N/35°W	-*	-*	36	doi:10.1594/PANGAEA.869653 | 869651
Sonne 171 (May-Jun 2003)	06BE20030 525	6°S-7°N/35°W	34	34	34	doi:10.1594/PANGAEA.742995 | 873268
Maurice Ewing CITHER2 (Jan-Mar 1994)	323019940 104	13°S-2°S/31°W-30°W	27	27	-	https://cchdo.ucsd.edu/cruise/3230CITHER2_1**
Hesperides FICARAM15/1 (Mar-May 2013)	29HE20130 320	13°S-0°/30°W	16	16	-	https://cchdo.ucsd.edu/cruise/29HE20130320**
Sonne 170 (Apr-May 2003)	06BE20030 423	12°S-3°S/28.5°W	16	16	16	doi:10.1594/PANGAEA.869338 | 869641
Meteor 53/2 (Jan-Feb 2002)	06M32002 0506	12°S-2.5°N/28°W	-*	-*	32	doi:10.1594/PANGAEA.869653 | 869651
Melville HYDROS4 (Mar-Apr 1989)	318M1989 0313	15°S-1°N/25°W	30	30	-	https://cchdo.ucsd.edu/cruise/318MHYDROS4**
Malcom Baldridge (Jul-Aug 1991)	33MW199 10711	15°S-5°N/25°W	13	13	-	https://cchdo.ucsd.edu/cruise/3175MB91**
Malcom Baldridge (Jul 1993)	33MW199 30704	5°S-5°N/25°W	16	16	-	https://cchdo.ucsd.edu/cruise/3175MB93**
Ronald H. Brown (Jun-Jul 2003)	33RO2003 0619	6°S-3°N/25°W	25	25	23	https://cchdo.ucsd.edu/cruise/33RO200306_01; http://currents.soest.hawaii.edu/clivar/ladcp/A16N/table0.html
Ronald H. Brown (Jan-Feb 2005)	33RO2005 0111	15°S-2°S/25°W	27	27	-	https://cchdo.ucsd.edu/cruise/33RO200501**
Ronald H. Brown (Aug-Oct 2013)	33RO2013 0803	6°S-3°N/25°W	25	25	-	https://cchdo.ucsd.edu/cruise/33RO20130803**
Ronald H. Brown (Dec-Jan 2013)	33RO2013 1223	15°S-6°S/25°W	17	17	-	https://cchdo.ucsd.edu/cruise/33RO20131223**
Thalassa EQUALANT99 (Sep-Oct 1999)	35TH19990 712	7°S-7°N/23°W	44	44	26	https://cchdo.ucsd.edu/cruise/35THEQUALANT9907
Meteor 47/1 (Mar-Apr 2000)	06M32000 0316	5°S-4°N/23°W	25	25	24	doi:10.1594/PANGAEA.787872 | 873266
Meteor 80/1 (Oct-Nov 2009)	06M32009 1026	5°S-15°N/23°W	76	76	75	doi:10.1594/PANGAEA.777865 | 811718
Maria S. Merian 18/2 (May-Jun 2011)	06MM201 10511	5°S-12°N/23°W	37	37	31	doi:10.1594/PANGAEA.783349 | 846777

Maria S. Merian 22/1 (Oct-Nov 2012)	06MM20121024	5°S-15°N/23°W	70	70	49	doi:10.1594/PANGAEA.830253 | 846763
Meteor 106/1 (Apr-May 2014)	06M320140419	8°S-15°N/23°W	72	72	58	doi:10.1594/PANGAEA.869361 | 869634
Knorr 142/3 (Apr-May 1994)	316N19940403	15°S-7.5°N/19°W	47	47	-	https://cchdo.ucsd.edu/cruise/316N142_3**
Meteor 14/2 (Oct 1990)	06M319901001	35°W-32.5°W/5.65-5°S	9	9	5 (only Pegasus)	doi:10.1594/PANGAEA.290710 | 873335
Meteor 16/3 (May-Jun 1991)	06M319910523	35°W-32°W/5.65-5°S	11	11	6 (only Pegasus)	doi:10.1594/PANGAEA.290711 | 873388
Meteor 22/2 (Oct-Nov 1992)	06M319921023	35°W-30°W/5.65-5°S	15	15	8 (only Pegasus)	doi:10.1594/PANGAEA.290713 | 873389
L'Atalante CITHER1 (Feb 1993)	35A31993010 2	35°W-23°W/5.65-4.5°S	25	25	-	https://cchdo.ucsd.edu/cruise/35A3CITHER1_1**
Meteor 27/3 (Feb-Mar 1994)	06M319940206	35°W-31.5°W/5.65-5°S	12	12	12	doi:10.1594/PANGAEA. 290714 | 319330
Thalassa EQUALANT99 (Sep-Oct 1999)	35TH19990712	35°W-30°W/5.65-5°S	13	13	6	https://cchdo.ucsd.edu/cruise/35THEQUALANT9907
Meteor 47/1 (Mar-Apr 2000)	06M320000316	35°W-23°W/5.65-5°S	31	31	30	doi:10.1594/PANGAEA.787872 | 873266
Sonne 151 (Nov 2000)	06BE20001103	35°W-32°W/5.65-5°S	13	13	13	doi:10.1594/PANGAEA.869339 | 869645
Meteor 53/2 (Jan-Feb 2002)	06M320020506	35°W-29°W/5.65-5°S	-*	-*	18	doi:10.1594/PANGAEA.869653 | 869651
Sonne 170 (Apr-May 2003)	06BE20030423	35°W-29.5°W/5.65-5°S	17	17	17	doi:10.1594/PANGAEA.869338 | 869641
Meteor 62/2 (Aug 2004)	06M320040808	35°W-30°W/5.65-5°S	13	-	12	doi:10.1594/PANGAEA.869654 | 869655
Meteor 98/1 (Jul 2013)	06M320130701	35°W-32°W/5.65-5°S	12	12	12	doi.10.1594/PANGAEA.868640 | 873265
Meteor 106/1 (Apr-May 2014)	06M320140419	35°W-31.5°W/5.65-5°S	16	16	13	doi:10.1594/PANGAEA.869361 | 869634
Meteor 22/2 (Oct-Nov 1992)	06M319921023	35.5°W-32.5°W/10°S	10	10	-	doi:10.1594/PANGAEA.290713

Meteor 27/3 (Feb-Mar 1994)	06M31994 0206	35.5°W-32°W/10°S	14	14	14	doi:10.1594/PANGAEA. 290714 | 319330
Meteor 28/1 (Mar-May 1994)	06M31994 0329	36°W-23°W/10°S-11.35°S	30	30	-	doi:10.1594/PANGAEA.293946
Meteor 47/1 (Mar-Apr 2000)	06M32000 0316	36°W-31.75°W/10.25°S-11.5°S	16	16	17	doi:10.1594/PANGAEA.787872 | 873266
Sonne 151 (Nov 2000)	06BE20001 103	36°W-31.75°W/10.25°S-11.5°S	22	22	22	doi:10.1594/PANGAEA.869339 | 869645
Meteor 53/2 (Jan-Feb 2002)	06M32002 0506	36°W-28.5°W/10.25-11.7°S	-*	-*	13	doi:10.1594/PANGAEA.869653 | 869651
Sonne 170 (Apr-May 2003)	06BE20030 423	36°W-28.5°W/10.25°S-11.5°S	26	26	26	doi:10.1594/PANGAEA.869338 | 869641
Meteor 62/2 (Aug 2004)	06M32004 0808	36°W-31°W/10.25°S-11.5°S	19	-	19	doi:10.1594/PANGAEA.869654 | 869655
Meteor 98/1 (Jul 2013)	06M32013 0701	36°W-32°W/10.25°S-11.5°S	21	21	21	doi.10.1594/PANGAEA.868640 | 873265
Meteor 106/1 (Apr-May 2014)	06M32014 0419	36°W-32°W/10.25°S-11.5°S	22	22	21	doi:10.1594/PANGAEA.869361 | 869634

For all of the used ship sections, deep profiles of *in-situ* temperature and salinity measured with a conductivity-temperature-depth (CTD) system are available. Dissolved oxygen was measured at about 95% of the stations. For early cruises (pre 1994) aboard R/V Meteor, Rhein et al. (1995) estimated temperature accuracy to be 0.002 – 0.004 °C, salinity accuracy on the order of 0.003 and oxygen accuracy of the calibrated sensor at 0.15 ml l^{-1} (about 6.7 µmol kg^{-1}). The accuracy of CTD data from cruises between 1990 – 2004 analyzed by Schott et al. (2005) was 0.002 – 0.003 °C for temperature and 0.002 – 0.0025 for salinity. Hydrography data from the cruise "Meteor 53/2" are not used because calibration of the CTD could not be performed with the required accuracy. For all other cruises we assume the accuracy of any data point to fall within the WOCE standard for water samples (e.g., WOCE Operations Manual, 1991).

Direct velocity profiles are available for about 67% of all used stations. From some of the early Meteor cruises (pre 1994), Pegasus velocity profiles are used (Table 2) which measure velocities with an accuracy of 1 cm s^{-1} by surveying the position of a free-falling float with acoustic bottom transponders (Spain et al., 1981; Schott et al., 2005). During later cruises, a 150-kHz narrowband Acoustic Doppler Current Profiler (ADCP) had been mounted routinely on the CTD rosette sampler. During most cruises

since 2004, a combination of an upward and downward looking 300-kHz ADCP was used. A detailed description of the technique and processing of the LADCP is given by Fischer and Visbeck (1993). The accuracy of the LADCP data is usually assumed to be about 4 - 5 cm s^{-1} (e.g., Schott et al., 2005).

The bathymetry shown in several figures is based on bathymetric data from the ETOPO1 Ice Surface dataset. ETOPO1 is a 1 arc-minute global relief model of Earth's surface integrating land topography and ocean bathymetry that was built from numerous global and regional datasets (Amante and Eakins, 2009).

2.2 Methods

Profiles of potential temperature (θ) in [°C], salinity (S) in [], dissolved oxygen (O_2) in [µmol kg^{-1}], zonal and meridional velocities (u, v) in [cm s^{-1}] for each section are sorted into 3D-matrices with 0.05° horizontal and 10 dbar vertical resolution. The third dimension is time, which, for all profiles taken during an individual ship survey, is the mean day of the measurements. For analyses of time-averaged fields, the variables are linearly interpolated between the profiles of the individual ship surveys at each depth level. A Gaussian-shaped weighting function, with horizontal and vertical influence and cut-off radii of 0.1° and 20 dbar and 0.25° and 30 dbar for meridional sections and 0.1° and 30 dbar and 0.3° and 50 dbar for zonal sections, respectively, is further applied for extrapolation and smoothing. The mapping scales are chosen to be as small as possible, but - for better visualization - allow a smoothing of excessive gradients due to irregular distribution of measurements.

The dataset analyzed in this study, consisting of different shipboard sections, has a reasonable horizontal two-dimensional coverage to visualize mean water mass properties on isopycnal surfaces in geographical maps. Within these maps, all available station data were included, thus combining data from different periods, from well-sampled repeated sections, and from one-time sections. Maps of AABW properties could be biased towards interior ocean values in regions where isopycnals intersect with the bathymetry. Mean potential temperature θ [°C] on neutral density (γ^n-) surfaces, representing the core depths of mNADW, lNADW, lighter and denser AABW, is shown together with transports within the individual layers to illustrate their mean pathways. Transports per 0.05° latitude or longitude in m^2 s^{-1} are calculated for section parts which were measured at least three times, from the interpolated fields of the current component normal to the sections for each individual cruise. For the four density layers, velocity is averaged vertically between the two corresponding isopycnal water mass boundaries (or between the isopycnal and the bottom) and then multiplied by the layer height. The local orientation of the sections is accounted for by calculating the cross-sectional velocity component.

For the calculation of trends, linear regression is applied using the least squares method (cf. Emery and Thompson, 2004; p. 1556 – 1567). With only a few realizations at each location (up to a maximum of 13 for the 5°S section – see Figure 2), it would be unreasonable to expect robust statistics. Therefore, mean

values should be taken as an indication of typical conditions and trends for any linear evolution. We argue that any spatial consistency between local results increases our confidence and justifies the application of this method. Hence we combine local results for a larger, dynamically connected region – the northern Brazil Basin – and thereby generate a time series with 32 realizations spanning 26 years. Linear trend values in this study, defined as the slope m_i of the regression (where the index i denotes the different parameters), are always stated as change per year in [$\cdot 10^{-3}$ °C yr^{-1}] for temperature and in [dbar yr^{-1}] for pressure. The standard error of the slope multiplied by 1.96 is specified as the 95% confidence interval estimate. We account for property changes on isobaric surfaces due to the combined effects of changes along isopycnal surfaces, intrinsic water mass changes, and vertical displacement of the isopycnals (Bindoff and McDougall, 1994). Therefore, we separately show trends calculated on pressure levels and on neutral density surfaces. The linear trends are fitted to temperature or pressure anomalies on mean pressure- or γ^n-surfaces which are horizontally smoothed with a median-filter[3], and anomalies from the 1999 – 2004 time average. Trends are calculated only if at least 4 realizations were available. To account for data coverage and spatial changes in the depth of the corresponding γ^n-surface along the sections, the anomalies are weighted with the number of measurements per time step and region, and linear trends are fitted individually for specific regions – the EQCH (along 35°W between 6°S – 1°N), the whole northern Brazil Basin (combining measurements along 11°S, 5°S, 25°W and 23°W, but only south of 1°S) and the VCH (between 40°W – 36°W).

3. MEAN HYDROGRAPHY AND WATER MASS DEFINITIONS

Neutral density, γ^n (in kg m^{-3}), allows a more consistent water mass separation compared to the traditional use of potential density. In this study, the CSIRO software by Jackett and McDougall (1997) is used to calculate 43 specific γ^n-surfaces for each section spanning eight neutral density layers. Those layers are chosen depending on the local water mass distributions described below, as well as to fit earlier water mass definitions with the potential density surfaces used by Schott et al. (2003, 2005). An additional subdivision of the deepest layers into a lighter and denser AABW is subjectively chosen by the authors and supported by the results of this study. It should be noted, that the water mass definitions vary widely among authors and for different regions. Table 3 summarizes our choices of γ^n-levels for boundaries and

[3] Mean and median filters are tools for noise suppression. While mean filtering is usually used to suppress Gaussian noise, median filtering is powerful when there is limited spatial data coverage, as it is less affected by outliers and skewness. The basic idea of this filtering technique consists of simultaneously replacing every data point with the median of all data points surrounding it in a specified radius (Yagou et al., 2002). Here, filter radii of five grid spaces along the four repeated sections and of two grid spaces for measurements within the VCH are chosen.

core depths of the water masses, as well as the choice of four other studies using neutral density to define deep water masses in the Brazil Basin (columns 6 – 9).

Figures 3-5 display sections of mean potential temperature (θ in °C) and mean dissolved oxygen (O_2 in μmol kg^{-1}) including mean salinity contours (S), which were derived by averaging all available sections from individual ship surveys. In the following, local NADW and AABW distributions are briefly reviewed together with the choice of subdividing isopycnals.

Table 3 Isopycnal surfaces defining eight water mass layers. These are the same layers as those used by Schott et al. (2003, 2005) defined by potential density (σ) surfaces (column 6), but are defined by neutral density surfaces instead. The "Water mass ID" column shows the name given to layers and water masses (SACW = South Atlantic Central Water, AAIW = Antarctic Intermediate Water, uCDW = upper Circumpolar Deep Water, NADW = North Atlantic Deep Water where the u, m or the l refer to upper, middle and lower branches, and AABW = Antarctic Bottom Water). A subdivision of the deepest layers into a lighter and denser AABW is subjectively chosen. Column 5 gives the number of equally spaced γ^n-levels spanning each layer. Columns 7 – 9 summarize the choice of water mass boundaries of other studies focusing on the Brazil Basin.

Layer	Water mass ID	γ^n [kg m^{-3}] water mass boundaries	γ^n [kg m^{-3}] water mass cores	Levels	σ [kg m^{-3}] along 35°W, 5°S, 11°S Schott et al. (2003, 2005)	γ^n [kg m^{-3}] along 19°S Vanicek & Siedler (2002)*	γ^n [kg m^{-3}] along 30°W Morris et al. (2001)**	γ^n [kg m^{-3}] along 11°S Ganachaud (2003)
1	surface waters	24.448			24.5 (σ_θ)	26.6		
2	SACW	26.8715			26.8 (σ_θ)	27.15		27.3
3	AAIW & uCDW	27.7153			32.15 (σ_1)	27.75		27.5
4	uNADW	28.0225	27.9	8	37 (σ_2)	27.98		27.97
5	mNADW	28.0931	28.06	8	45.83 (σ_4)	28.03 28.07		28.07
6	lNADW	28.135	28.11	8	45.9 (σ_4)	28.12	28.133	28.11
7	lighter AABW	> 28.225	28.17	10		28.24	28.16 28.205	
8	denser AABW		28.25	7			28.27	

*In this study, NADW was subdivided into four layers following Rhein et al. (1995).

**Morris et al. (2001) subdivided AABW into four layers, with the neutral density surfaces chosen to coincide with the 0°, 0.8°, 1.2° and 1.6°C isotherms in the Vema Channel. But the authors also pointed out that those interfaces diverge in the interior of the basin and farther north.

The interface between NADW and the intermediate waters above is defined by γ^n = 27.715 kg m^{-3}, approximately coincides with the 180 µmol kg^{-1} isoline for oxygen and lies in between the choices of Vanicek and Siedler (2002) along 19°S and Ganachaud (2003) along 11°S. In all five sections in Figures 3-5, NADW covers a thick layer ranging from about 1200 to 4000 dbar and is generally characterized by high oxygen concentrations and a relative salinity maximum. Along the equator, the property distribution allows for an additional subdivision into at least three layers of different origin. A salinity maximum and high oxygen concentrations are indicators for the uNADW in the tropical Atlantic. Upon entering the Brazil Basin, the pronounced salinity maximum is located slightly above the shallow oxygen maximum (Figure 3b). Farther south this vertical structure becomes less clear. Here, the lower boundary of the uNADW is chosen to be 28.023 kg m^{-3} and is typically found at 2330 – 2400 dbar. Maxima of O_2 (> 260 µmol kg^{-1}) reaching down to about 4000 dbar in the western boundary region also characterize the mNADW and lNADW layers. Those are typically more pronounced in the western parts of the 5°S, 11°S sections (Figures 5b,d) and in the southern part of the 35°W section (Figure 3b), compared to an offshore decrease in oxygen. The latter is probably caused by contributions of "older" NADW recirculating (e.g., Friedrichs et al., 1994; Rhein et al., 1995).

Following Schott et al. (2003; 2005), we decided to separate the mNADW from the lNADW by the γ^n = 28.093 kg m^{-3} isopycnal. In part continuing to flow along the western boundary, the mNADW and lNADW seem to be strongly transformed there. From the 35°W section (Figure 3b) towards the 5°S section (Figure 5b), the former confined O_2 maximum is reduced and evenly distributed over a broader region. From 5°S to 11°S (Figure 5d), the O_2 maximum is further reduced and lifted upward towards shallower depths. Concurrently, the O_2 maxima of the NADW layers can be followed in a confined band along the equator to 25°W (Figure 3d, between 0° and 2°S) and are even found at the entrances to the RCHFZ at 23°W (Figure 4b, between 0° and 2°S). This supports the assumption that for at least some parts of the NADW the eastward pathway along the equator is given equal preference to the southward one with the DWBC (e.g., Richardson and Fratantoni,1999; Rhein et al., 2015). Along the two meridional sections in the eastern part of the Brazil Basin, we additionally observe a pronounced oxygen minimum sandwiched between the shallow and deep O_2 maxima of the NADW which occupies the density range of the mNADW. This oxygen pattern in the NADW layers, becoming more pronounced from the 35°W section towards the 23°W section, could be the signature of another water mass filling the mNADW density away from the western boundary. Interestingly enough, the 25°W and 23°W sections show two additional bands with a similar vertical structure in oxygen farther south - at 4-6°S (Figures 3d and 4b)

and 9-11°S (shown only in Figure 3d). The location of these bands qualitatively agrees with the location of basin-wide nearly barotropic eastward jets that have been observed in ship sections along 23°W (e.g., Gouriou et al., 2001; Greatbatch et al., 2012) and were found in mean velocity distribution from Argo floats drifting at 1000 dbar (see e.g., Figure 2 in Ascani et al., 2010).

Below 4000 – 4500 dbar, lower values of salinity ($S < 34.85$), potential temperature ($\theta < 1.8$ °C) and dissolved oxygen ($O_2 < 260$ µmol kg^{-1} in the western part of the basin, $O_2 < 250$ µmol kg^{-1} south of the equator at 25°W and 23°W) indicate the presence of AABW in the entire northern Brazil Basin. All properties decrease almost linearly with depth. While many studies adapted the traditional choices of the 2 °C isotherm as the boundary between the NADW and AABW, we define it by the $\gamma^n = 28.135$ kg m^{-3} isopycnal, which coincides with θ about 1.7 to 1.8 °C and O_2 about 250 to 260 µmol kg^{-1} isolines along all four sections in the northern Brazil Basin. Our choice is within the range of existing studies which also use neutral density and focus on the Brazil Basin (e.g., Morris et al., 2001; Vanicek and Siedler, 2002; Ganachaud, 2003; see Table 3), and which particularly describe the situation in the northern Brazil Basin.

As discussed in chapter 1, the AABW in the Atlantic sector is thought to be a mixture of LCPW and WSDW. In the VCH, Zenk and Visbeck (2013) separated the WSDW at the bottom by the 0.2 °C isotherm from the LCPW above, which is a definition adopted from Speer and Zenk (1993). It is assumed, that the LCPW fraction is larger in the Brazil Basin compared to WSDW (e.g., Mantyla and Reid, 1983). The formation process of LCPW includes upwelled old deep water that is already depleted in O_2. In fact, the LCPW dominance in the Brazil Basin explains the lower oxygen concentrations found within all AABW layers in the investigated region. Within the EQCH, mean potential temperatures of the AABW range from 0.55 – 1.8 °C (Figure 3a), while temperature values down to 0.2 °C can only be found in deeper, more interior parts of the Brazil Basin along 5°S and 11°S (Figure 5a,c). At 25°W (Figure 3c) and 23°W (Figure 4a), more homogenized AABW with minimum temperatures of 0.4 °C fills deep levels at the foot of the MAR south of 1°S.

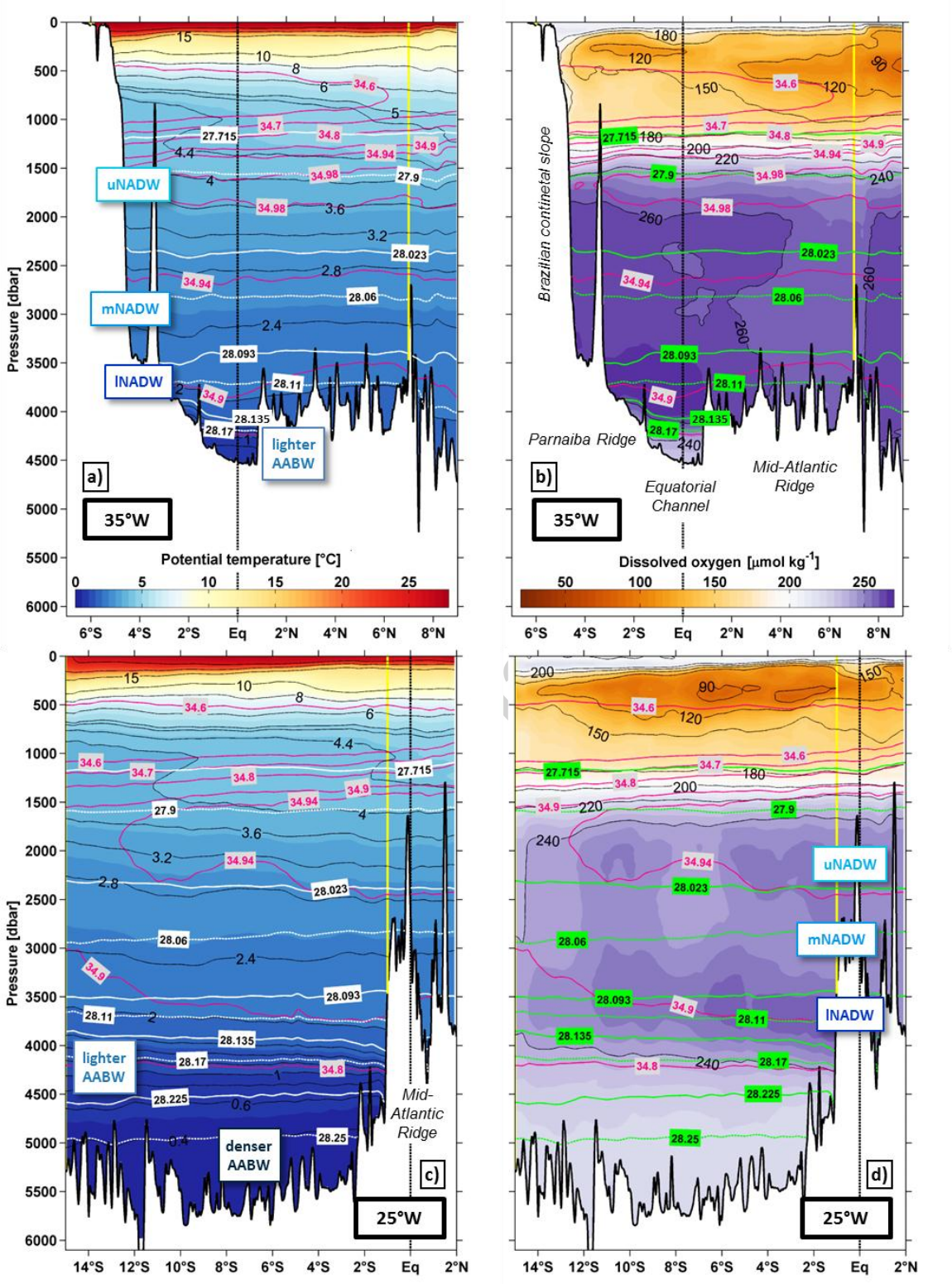

Figure 3 Vertical sections of θ [°C] and O_2 [µmol kg^{-1}] along 35°W and 25°W, averaged over 12 and 7 cruises, respectively. White or green contours mark neutral density levels γ_n [kg m^{-3}] defining water mass boundaries (solid) and cores (dashed) of the NADW and AABW layers. Mean salinity is shown by selected contours in magenta. Relevant water masses are indicated by their abbreviations (compare Table 3). Vertical yellow lines separate regions with clear differences in data coverage.

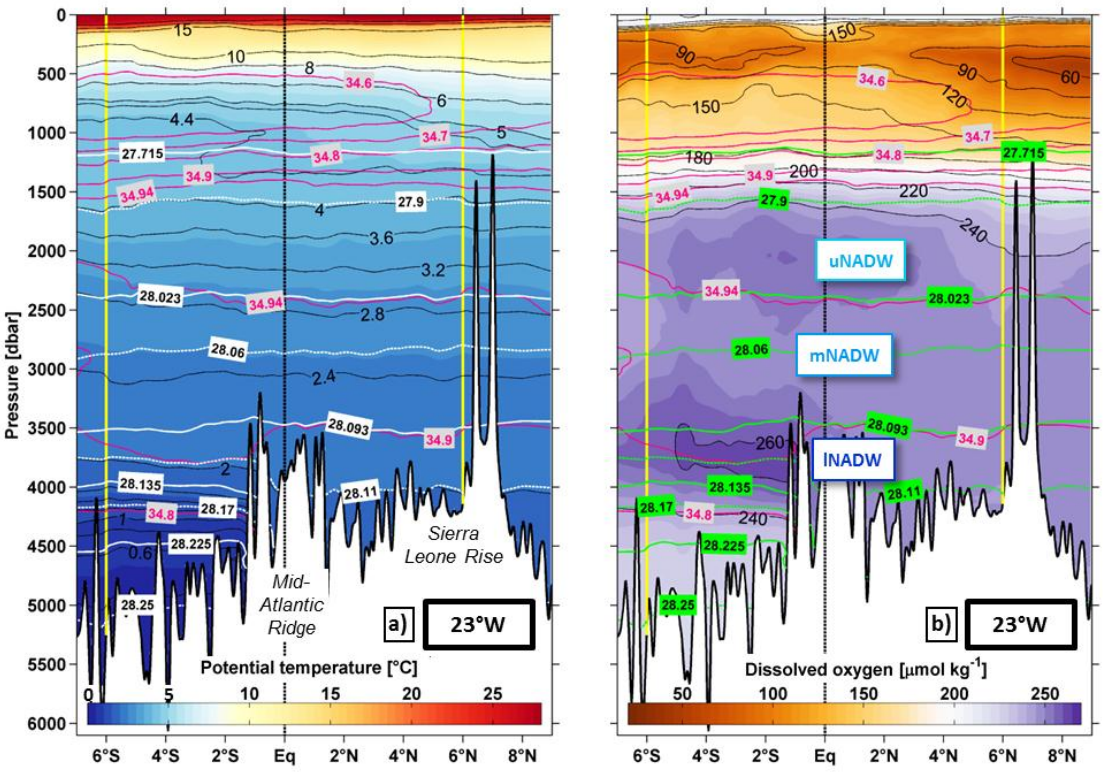

Figure 4 Same as Figure 3, but along 23°W, averaged over 6 cruises.

This rather suggests that the denser component of the AABW, if still present at those latitudes, circulates in the interior of the northern Brazil Basin at levels deeper 4500 – 4700 dbar. It does not pass through the EQCH into the western North Atlantic. We choose the γ^n = 28.225 kg m^{-3} isopycnal to separate a lighter from a denser AABW component in the northern Brazil Basin since we observe different behavior for the layers above and below that isopycnal (see chapter 5). In the tropical Atlantic this isopycnal typically coincides approximately with the 0.6 °C isotherm.

4. SPATIAL PROPERTY CHANGES

4.1 Temperature distributions on isopycnals and mean pathways

While at fixed depth, variations in water mass properties can be caused by internal waves or eddies and the associated vertical displacements of isopycnal surfaces, an analysis in a neutral density frame work leads to a separation of water mass modifications from isopycnal heave (e.g., Durack and Wijffels, 2010). In the following we will study mean pathways of deep and bottom water masses using the observed horizontal distributions in the θ-S-composition on isopycnal surfaces that correspond to changes in the spiciness induced by mixing of different water masses.

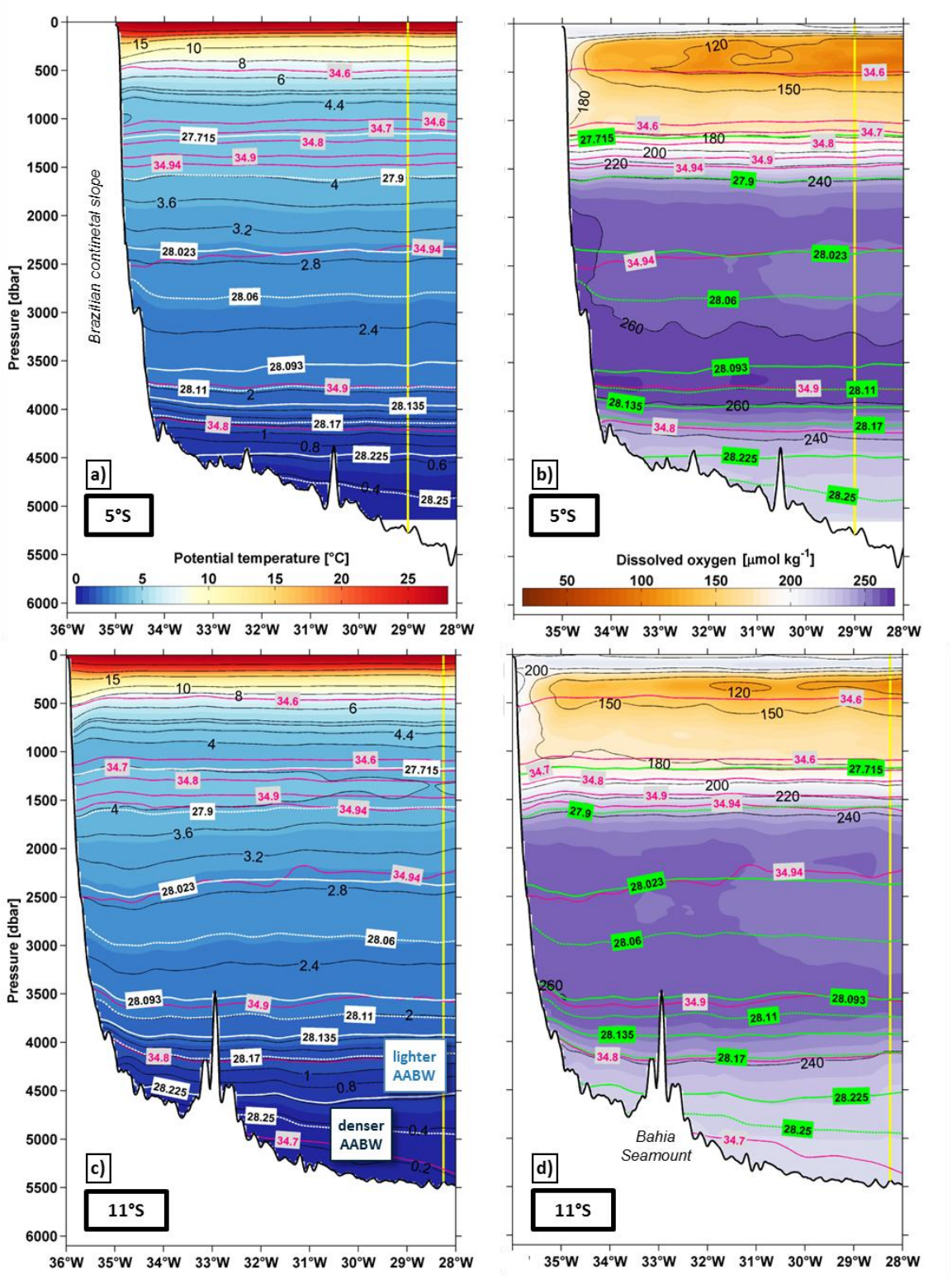

Figure 5 Same as Figure 3, but along 5°S and 11°S, averaged over 13 and 8 cruises, respectively.

The θ distributions on isopycnal surfaces representing the cores of mNADW and lNADW (Figure 6a,b) show relatively warm waters to enter the northern Brazil Basin at 35°W. This flow is concentrated in a well-defined current core at 1.5°S which is topographically guided by the Parnaiba Ridge. In the mNADW layer, the warmer waters can clearly be followed together with the velocity signal of the DWBC southward along the continental slope. At 5°S and 11°S we observe that the southward flow is limited by a northward recirculation farther offshore. The northward recirculation at 11°S was explained by the presence of southward migrating anticyclonic eddies which result from a break-up of the continuous DWBC south of about 8°S (Dengler et al., 2004). In the rest of the northern Brazil Basin, temperatures on the mNADW core isopycnal tend to be slightly cooler with patches of θ minima along the northern extension of the 4500 dbar contour or south of 6°S in the western basin. This distribution is in agreement with Friedrichs et al. (1994) who assumed older modified or recirculated water masses coming from the western boundary or southern Brazil Basin to contribute to the southward flow in the DWBC in the mNADW density range.

Away from the EQCH, the lNADW layer shows different behavior compared to the mNADW above. Here we find the lNADW and the lighter AABW components together to form an interactive transition layer with their temperature distributions on isopycnals (Figure 6b-c) gradually changing as both water masses experience mixing along their pathways. This can clearly be seen as the temperature on those isopycnals changes from the South towards the equator and from the western boundary towards the basin interior. Along the western boundary, the θ distributions on both isopycnal surfaces (of lNADW and lighter AABW) show rather lower temperatures at 5°S and rather higher temperatures at 11°S compared to the basin interior. This indicates that the strongest mixing between the lNADW and lighter AABW happens along this particular route. The distributions also show warmer temperatures on both isopycnal surfaces along the equator, which we interpret as the warmer lNADW being the more dominant water mass in that density range north of 5°S and throughout the entire width of the basin. While from the 35°W section towards the 5°S section the transport of lNADW drastically decreases, we can observe an eastward current band at 2-3°S at the 23°W section which reaches down into the lNADW layers. This is interpreted as an eastward extension not only of the upper NADW but also of the lNADW (e.g., Gouriou et al., 2001), flowing parallel to the equator, and may partly explain the fate of large lNADW fractions off Brazil.

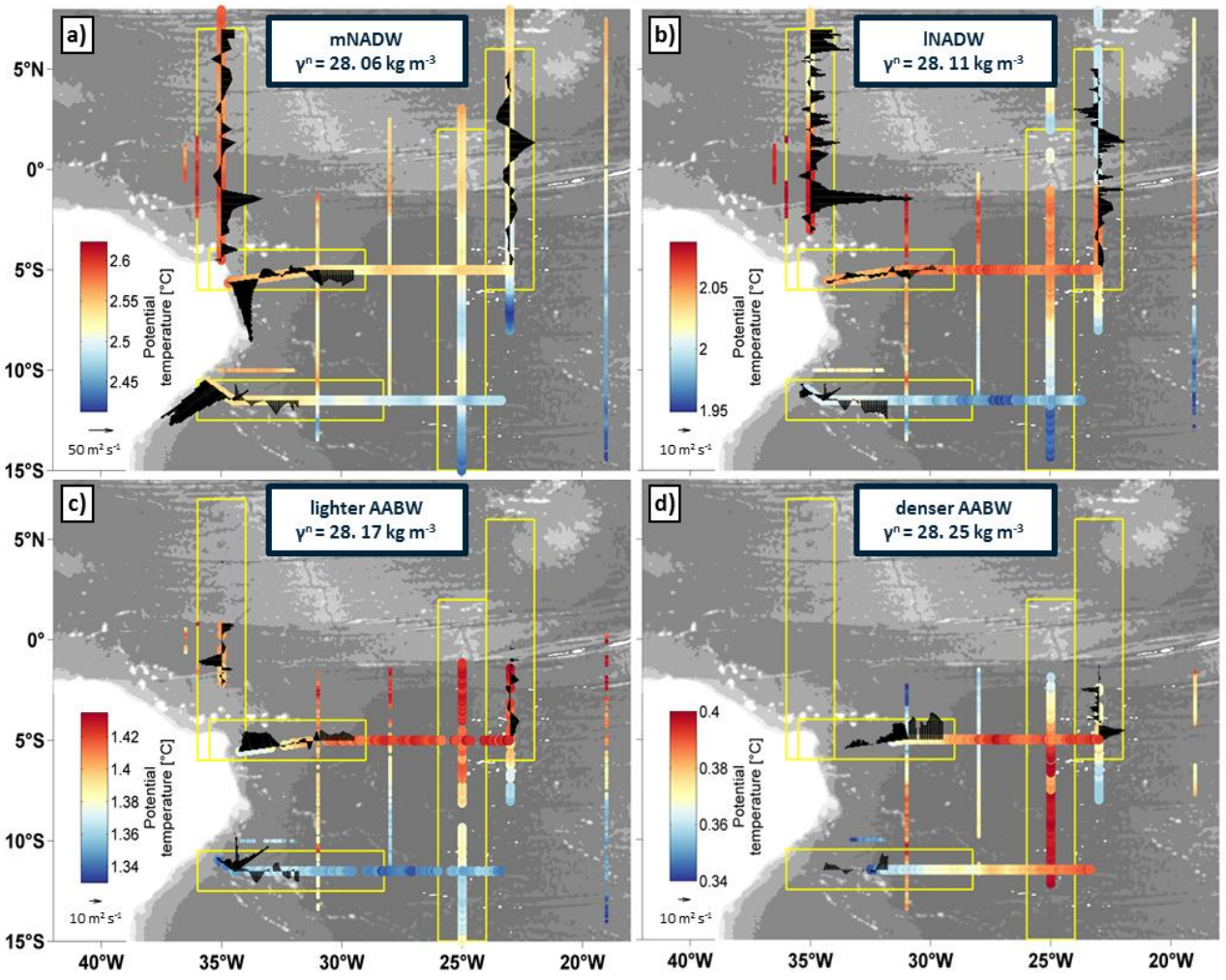

Figure 6 Potential temperature θ [°C] on neutral density surfaces, representing the core depth of the mNADW (a), lNADW (b), lighter AABW (c) and denser AABW (d). Black stick vectors mark velocities normal to each section integrated over the layer height [m^2 s^{-1}] for section parts which were measured at least three times. Note, that the color ranges and the reference stick vectors differ between water masses. Yellow boxes indicate section parts with better data coverage (compare with Figures 2-5). Grey contouring in the background shows ETOPO1 bathymetry (with contour intervals of 1000 m).

In the central and eastern interior parts of the basin (south of 5°S), lower temperatures are found on both isopycnal surfaces of lNADW and lighter AABW, indicating the dominant presence of AABW there. When examining the mean potential temperature together with the mean flow (Figure 6c), we see the northward transport of AABW to be partly confined along the western boundary just below the DWBC. This route rather transports the lighter component of the AABW, with transports being quite similar between the zonal sections, which makes this route one possible candidate for feeding the flow of AABW into the North Atlantic via the EQCH. Within the EQCH, we typically find the lowest temperatures within its deeper, more northern parts, although it seems that the AABW flow is more concentrated at its southern edge, confirming previous observations by Rhein et al. (1995, 1998). On the isopycnal surface

representing the core of dense AABW (Figure 6d), one can immediately see that those densities are confined to the deepest parts of the basin and are not found close to the western boundary or in the EQCH. From the mean current distribution we see that the denser component and also larger amount of AABW seems to propagate northward in the more interior parts of the basin along the 4500 dbar contour. Unfortunately, there the abyssal layers were barely sampled by the ship sections. Lower temperatures just east or south of the 4500 dbar contour along 11°S, 5°S, 25°W and 23°W confirm a spreading of the densest AABW restricted by topography – first flowing northward parallel to the Brazilian shelf and then turning east at about 5°S. Pronounced temperature minima at the northern end of 31°W section and along 10°S should be interpreted with care as those sections were measured in the early 1990s once or twice, when temperatures on isopycnals were noticeably lower compared to long-term averages for the repeated sections. From O_2 distributions we see that the AABW fills the deep levels south of 1°S (compare Figure 3-4), thus reaching the entrances of the RCHFZ. In the mean velocity fields along 23°W, however, no pronounced velocity core is found at the right location that could support eastward transport of AABW into the East Atlantic. Instead, we observe several westward velocity bands in the dense AABW between 1°S and 4°S, as well as a confined southeastward flow at 4-5°S. This might be a hint towards the AABW turning southward in this region. The westward flow was observed before by Hogg and Owens (1999) who analyzed float trajectories at 4000 m depth and found all floats in the northern half of the basin "as though coming out of the ridge". They interpret this to be the result of enhanced mixing over the MAR, diffusively driving an accompanying secondary circulation.

4.2 Water mass transformation along the major pathways

Upon arriving at the entrances to the Brazil Basin, the two denser NADW components and the AABW have already undergone strong modifications. Figure 7 displays θ-S-diagrams including hydrographic data from all ship sections mapped in Figure 2f for the density ranges of mNADW, lNADW and AABW. In the upper panel, the individual water masses are highlighted as they enter the basin: mNADW and lNADW through EQCH from the north in blue, AABW through VCH from the south in brown.

In the lower panel in Figure 7, all dots representing repeatedly measured locations along the 35°W, 25°W, 23°W, 5°S and 11°S sections are colored by the corresponding oxygen values to indicate how water masses change on their way through the northern Brazil Basin. For the mNADW, lNADW and lighter AABW, we observe the highest oxygen levels in the EQCH and a gradual decrease away from the EQCH.

As described in the previous chapter, we are able to identify and sample two major routes for the deep and bottom waters in this specific region – along the western boundary and parallel to the equator. In the following, transformation of mNADW, lNADW and AABW is investigated further by comparing θ-S-characteristics at different representative locations along each of the routes (Figures 8-9). Additionally, differences between the boundary region and the basin interior are disclosed along the 5°S section in Figure 10.

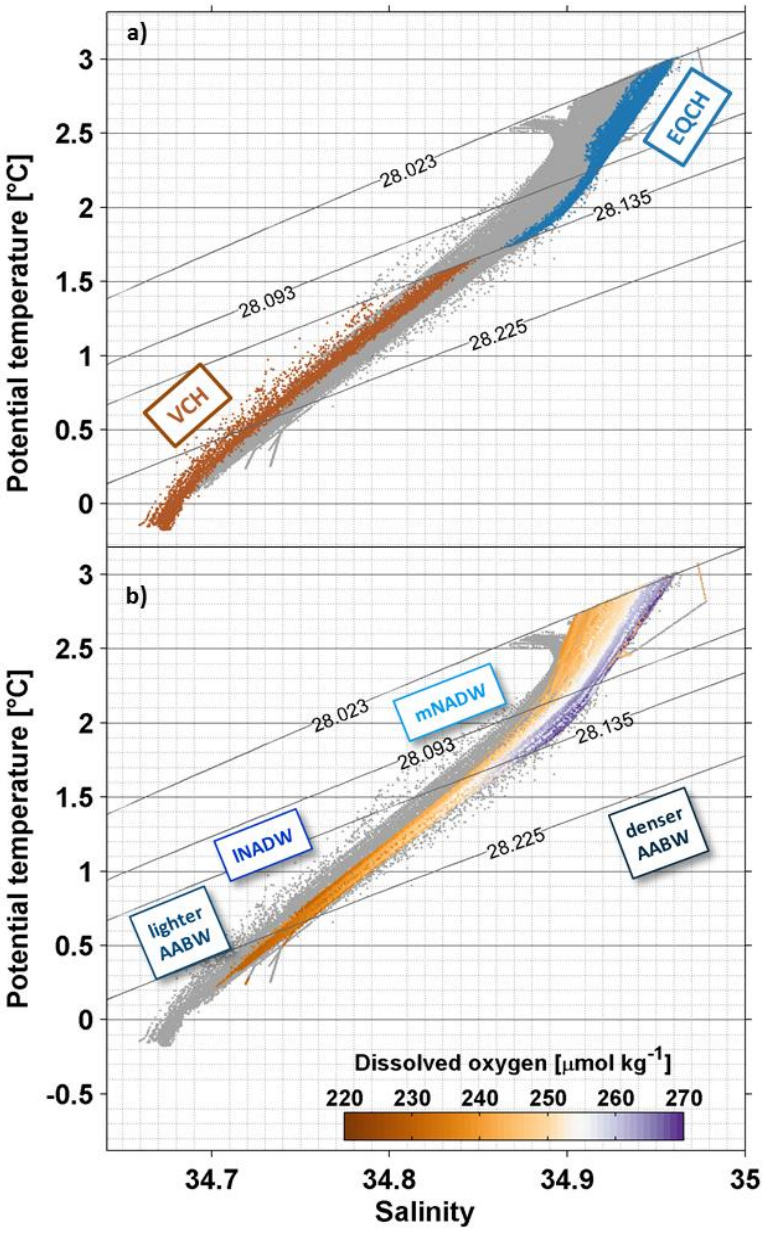

At 35°W (blue curves in Figures 8), the mNADW and lNADW layers enter the Brazil Basin with both having a more or less linear θ-S-relationship. Downstream of the DWBC (from the EQCH to 11°S and further to the VCH at 30°S), the NADW gradually freshens. The freshening is even more pronounced in the lNADW which is strongly transformed by interacting with the underlying AABW. As previously stated, we find the lNADW and lighter AABW components in the northern Brazil Basin to form a transition layer as they behave in a similar way. This is also supported by the lighter AABW which undergoes a comparable gradual salinification from South to North. The strongest modifications seem to occur just after the lNADW has crossed the equator, where we assume the presence of the Ceará Seamount Chain is one reason for enhanced mixing. Aside from the seamounts and enhanced internal wave activity, the shear between intensified western boundary currents in the NADW and AABW of opposite direction could also contribute to enhanced mixing along this pathway – with the combined effects possibly being strong enough to dilute the remaining lNADW characteristics in this region.

Between the 35°W section (dark blue curve in Figure 8) and the 5°S section (red curves in Figure 10), the salinity of the lNADW changes by ~0.008, and from 5°S towards 11°S (dark green curves in Figure 8) along the western boundary by ~0.009. A similar amount of salinity change (~0.02) occurs from 11°S towards 30°S (VCH; brown curves in Figure 8), over twice the distance.

Figure 7 θ-S-diagrams, including data from all available ship sections (grey dots), for the density ranges of mNADW, lNADW and AABW (γ^n > 28.023 kg m^{-3}; contours mark γ^n-levels defining water mass boundaries). a) Dots colored in blue or brown highlight measurements related to the mNADW and lNADW or AABW entering the Brazil Basin through the EQCH or VCH, respectively. b) Measurements from the repeated sections along 35°W, 25°W, 23°W, 5°S and 11°S are colored by the corresponding O_2 values.

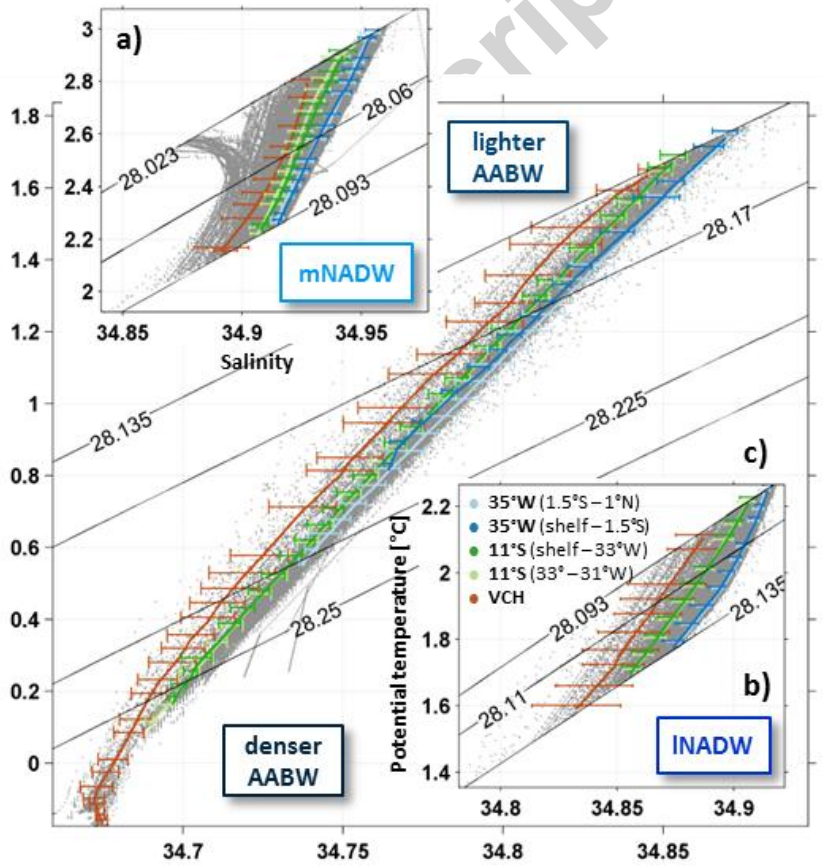

In the mNADW layer, salinity changes along the western boundary are also strongest between the 35°W section and the 5°S section (~0.007). This is the region where, in addition to enhanced mixing because of prominent topography, water masses from the southeastern Brazil Basin are proposed to join the flow at the western boundary within the same density range (e.g., Friedrichs et al., 1994; see chapter 1 and Figure 1). Between 5°S and 11°S, salinity changes by ~0.004, and between 11°S and 30°S by ~0.012.

Following the flow of NADW parallel to the equator (between 3°S – 2°N; orange and magenta curves in Figure 9), we observe that along this pathway freshening is similar in the mNADW to that along the western boundary. It is clearly weaker in the lNADW at about ~0.011 over 12° of longitude compared to ~0.017 over 11° of latitude. Weaker property changes along this route could be due to smoother

topography but also because the AABW has already being strongly transformed north of 5°S and flows into the same direction as the lNADW, resulting in weaker shear. The mNADW, on the other hand, is sandwiched between the uNADW and lNADW and mixing with those water masses at similar rates along both pathways.

Figure 8 θ-S-diagrams for the different density ranges of mNADW (28.0225 kg m^{-3} < γ^n < 28.0931 kg m^{-3}; a), lNADW (28.0931 kg m^{-3} < γ^n < 28.135 kg m^{-3}; b) and AABW (γ^n > 28.135 kg m^{-3}; c), following those water masses along the Brazilian coast in continuation of the DWBC. All data available from ship sections are shown with grey dots. Colored curves with errorbars are mean salinities and their standard deviations per density class. Color coding distinguishes between different regions and section parts along that path as listed in the legends. Contours mark γ^n-levels defining water mass boundaries.

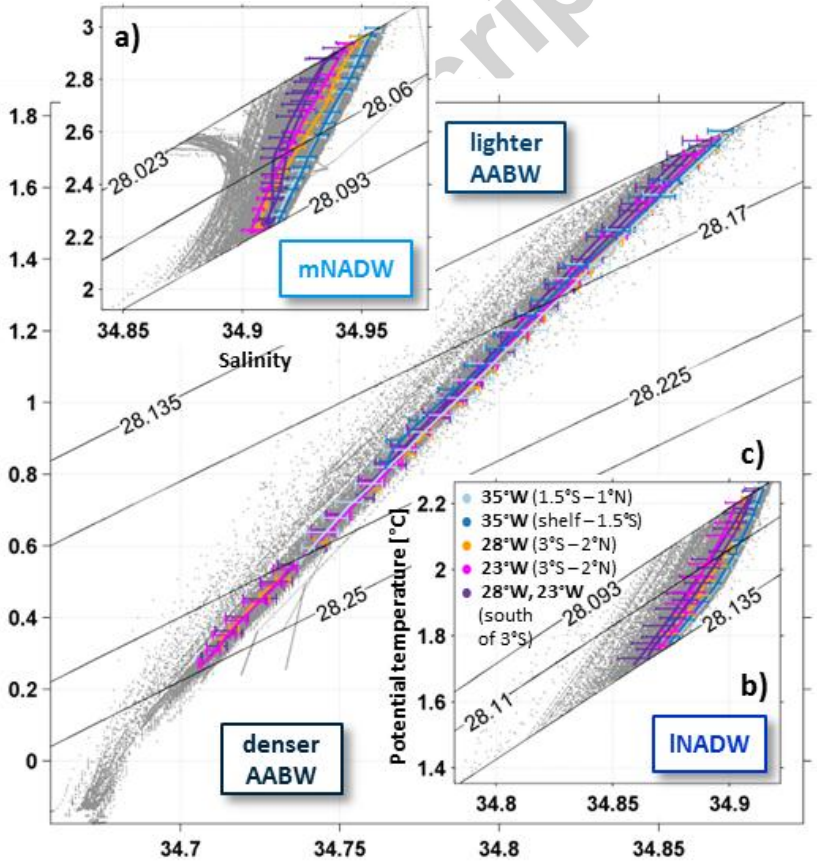

In the northwestern interior part of the Brazil Basin (south of 3°S in Figure 9 and east of 29°W in Figure 10), the lNADW shows very similar characteristics compared to the water mass transported along the equator. This supports our assertion that the lNADW fills all of the Brazil Basin north of 5°S at those densities as indicated before by the temperature distribution on the corresponding core isopycnal (Figure 6). Interestingly enough, the θ-S-relation in the mNADW density range in that region is rather S-shaped (dark purple curves in Figure 9). This can be interpreted as the result of another water mass entering the DWBC region from the southeastern Brazil Basin. There are competing hypotheses on the origin of this water mass, suggesting that it could be transformed lNADW returning as mNADW from the East Atlantic (Friedrichs et al., 1994) or "older" NADW recirculating from the western boundary region (e.g., Friedrichs et al., 1994; Rhein et al., 1995). At 30°S we find the mNADW layer to be occupied by remnants of NADW

arriving with the DWBC or the hook-shaped θ-S-profiles (grey dots forming a hook) characterizing the waters presumably entering through the HCH.

Figure 9 Same as figure 8, but combining meridional sections to follow the deep and bottom water layers along their eastward path parallel to the equator.

When the AABW enters the Brazil Basin through the VCH near 30°S (Figure 8), it features minimum temperatures of -0.18 °C and salinities of 34.66. Continuing northward it becomes more saline and warms by an equal amount as the lNADW freshens and cools, and, at the same time, loses its densest end-member in its mixing profile. We observe the lowest temperatures to gradually be lost following the western boundary from south to north, with -0.18 °C in the VCH, 0.11 °C at 11°S, 0.23 °C at 5°S and 0.55 °C in the EQCH. Unfortunately, our data set barely samples the coldest waters of the northern Brazil Basin which are mainly found in the deeper, more interior parts of the basin than along the continental slope – as can be seen along 11°S where lower temperatures by 0.1 °C were observed east of 33°W (light green curves in Figure 8). It may be of interest that at 5°S (light pink curves in Figure 10) the lowest temperatures are found in close vicinity to the 4500 dbar contour rather than farther east, highlighting this as the preferred route at that latitude compared to the basin interior east of 29°W. Along its denser path in the Brazil Basin, Mantyla and Reid (1983) found the downstream AABW characteristics over the latitude range from 30°S to the equator becoming similarly warmer by ~0.7 °C and saltier by ~0.07. Between 30°S and 4.5°S, Sandoval and Weatherly (2001) reported downstream AABW property variations smaller than 0.3 °C in potential temperature and 0.03 in salinity, which were roughly half smaller than those reported by Mantyla and Reid (1983).

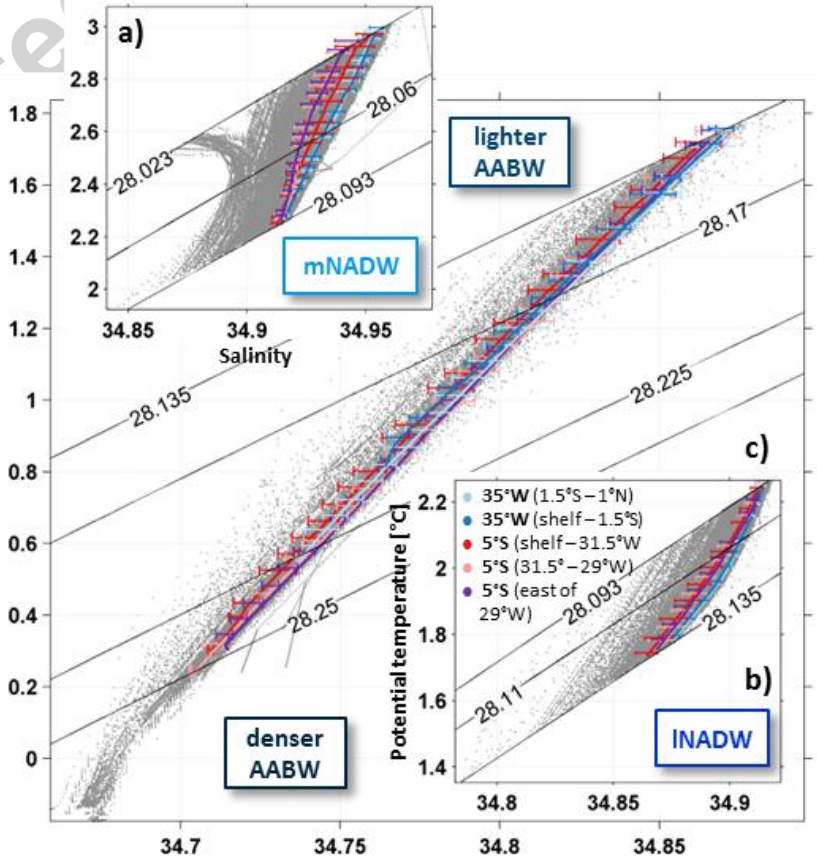

North of 5°S, the AABW following the western boundary northward is assumed to turn east as a contour-following current and to flow parallel to the equator towards the RCHFZ (e.g., Sandoval and Weatherly, 2001). Along the equatorial pathways we find the AABW to be much more homogenized and to have very

similar θ-S-characteristics everywhere east of 29°W and north of 5°S (additionally compare magenta, orange and purple curves in Figure 9). The cause for such homogenized AABW north of 5°S is not known, but could again be related to the existence of the Ceará seamount chain at about 4°S and associated stirring and mixing. In the EQCH, which represents the other route for the AABW to exit the Brazil Basin to the north, we do not observe AABW with $\gamma^n > 28.225$ kg m^{-3} (see also Figure 13). This means that only the lighter AABW component is able to pass through that channel and cross the equator. Additionally, we find differences in the θ-S-characteristics of AABW between the northern and southern parts of the channel (compare light and dark blue curves): The lowest temperatures (~0.55 °C) are measured in the northern half where the channel is deepest but velocities are sluggish and unsteady. At the same time, a pronounced westward velocity core found at the southern rim of the EQCH only transports waters with minimum temperatures of 0.8 °C.

Figure 10 Same as figure 8, but disclosing water masses further on their way from the equator towards and along the 5°S section.

5. LONG-TERM TEMPERATURE TRENDS

Spanning a period of 26 years, the dataset used can be treated approximately as a multi-decadal time series, allowing for the cautious estimation of long-term trends. In the following, we therefore investigate temporal temperature changes in the water mass properties of NADW and AABW arriving in the northern Brazil Basin from the North and the South with different approaches.

5.1 Evolution of the lowest temperatures in the Brazil Basin

From measurements in the VCH, Zenk and Morozov (2007) and Zenk and Visbeck (2013) found a decadal upward trend in the lowest temperatures. By analyzing only the lowest temperatures at three locations within the channel, the authors tried to capture the cold core of the WSDW which follows different pathways across the Rio Grande Rise. The evolution of these lowest temperatures showed a stagnant period over 20 years until 1990, followed by a significant temperature increase of $2 – 3 \cdot 10^{-3}$ °C yr^{-1} until 2006. Extending the time series until 2010 and finding it fully compatible with a three-year moored temperature series, Zenk and Visbeck (2013) confirmed a warming trend of almost $2 \cdot 10^{-3}$ °C yr^{-1}.

For direct comparison of this work with the results of Zenk and Morozov (2007) and Zenk and Visbeck (2013), we also investigate the lowest temperatures found along the five sections 35°W, 25°W, 23°W, 5°S, 11°S in terms of their temporal evolution. As a restriction, only temperature minima found within selected regions (colored shading in Figure 11b-f) are taken into consideration. The evolution of the lowest temperatures for each section, as well as the time series in VCH (brown curve), are displayed in

Figure 11a. The calculated trends are similar to those found by Zenk and Morozov (2007) or Zenk and Visbeck (2013) at 11°S (+2.8 ± 3.3 $\cdot 10^{-3}$ °C yr^{-1} for the period 1994 – 2014), at 25°W (+1.8 ± 0.7 $\cdot 10^{-3}$ °C yr^{-1} for the period 1989 – 2014) and at 23°W (+3.6 ± 5.0 $\cdot 10^{-3}$ °C yr^{-1} for the period 1999 – 2014), but up to two times larger at 5°S (+5.1 ± 5.4 $\cdot 10^{-3}$ °C yr^{-1} for the period 1990 – 2014) and 35°W (+5.8 ± 3.0 $\cdot 10^{-3}$ °C yr^{-1} for the period 1990 – 2003).

While at 11°S, 25°W and 23°W we are confident to mainly capture the dense AABW when restricting our analysis to the regions with high data coverage, the large positive trends at 5°S and 35°W should be put into perspective: As described in chapter 4, we find the 5°S section located in a region where strong water mass transformation occurs. At the same time we find the flows of lighter AABW along the continental slope (east of 31°W) and of denser AABW along the 4500 dbar isobar to merge or separate in this region. It means that we capture the lowest temperatures of both AABW versions depending on the different zonal extension of sections at different times, resulting in large variability. From chapter 4 we know that only the lighter AABW component is able to pass through the EQCH at 35°W and cross the equator. Therefore, we assume that along this section, with our approach, we are only able to capture the lighter AABW component. The large temperature changes at the bottom of the EQCH, the warming trends at 25°W from 1989 – 2014 and in the VCH from 1990 – 2010 are the only ones being different from zero when adding a 95% confidence estimate (highlighted with boxes around the number in Figure 11a). Overall, the warming of the coldest bottom waters is found to be of similar magnitude at all locations analyzed in the northern Brazil Basin and over different periods, which is in general agreement with findings of previous observational studies focusing on the same region (e.g., Johnson and Doney, 2006; Johnson et al., 2014).

5.2 Linear trends on isobars and isopycnals

To account for property changes on isobaric surfaces that are caused by intrinsic water mass changes or vertical displacement of isopycnals, the linear trends of θ for the lNADW and AABW layers in Figure 12 are shown separately on pressure levels and on isopycnal surfaces, as well as trends of pressure of the corresponding isopycnal surfaces. To increase reliability of the results, relevant measurements along 11°S, 5°S, 25°W and 23°W are combined to a single time series for the northern Brazil Basin, including 32 realizations and spanning 26 years. This is justified as we find those four section parts to be dynamically connected and to contain very similar AABW water mass properties (see chapter 4). For a better comparison with the time series in the EQCH, trends were calculated for subsets of the two longer time series over the period 1990 – 2003.

a) Warming of the denser AABW

The analysis on pressure levels reveals a warming of the densest AABW component throughout the period from 1989 to 2014 at about 2.5 ± 0.7 $\cdot 10^{-3}$ °C yr^{-1}. This warming is evident at all locations, uniformly distributed over the entire pressure range (below 4200 dbar in the northern Brazil Basin, Figure 12b, and 2.4 ± 1.1 $\cdot 10^{-3}$ °C yr^{-1} below 4300 dbar in the VCH, Figure 12c) and different from zero when adding a 95% confidence estimate. It is also in good agreement with temperature changes reported for the deep Brazil Basin by other studies, such as Johnson and Doney (2006) and Johnson et al. (2014). They detected a statistically significant warming trend of similar magnitude (2.4 – 4.4 $\cdot 10^{-3}$ °C yr^{-1} between 1989/1995 and 2005/2003 or 2 – 3 $\cdot 10^{-3}$ °C yr^{-1} from 1989 to 2014) on isobars in the most homogenous abyssal waters deeper than 4500 dbar and 4300 dbar, respectively. Johnson et al. (2014) found this region, along with the southern margins of the Argentine Basin and the Scotia Sea, to warm continuously over three occupations during the period 1989 to 2014.

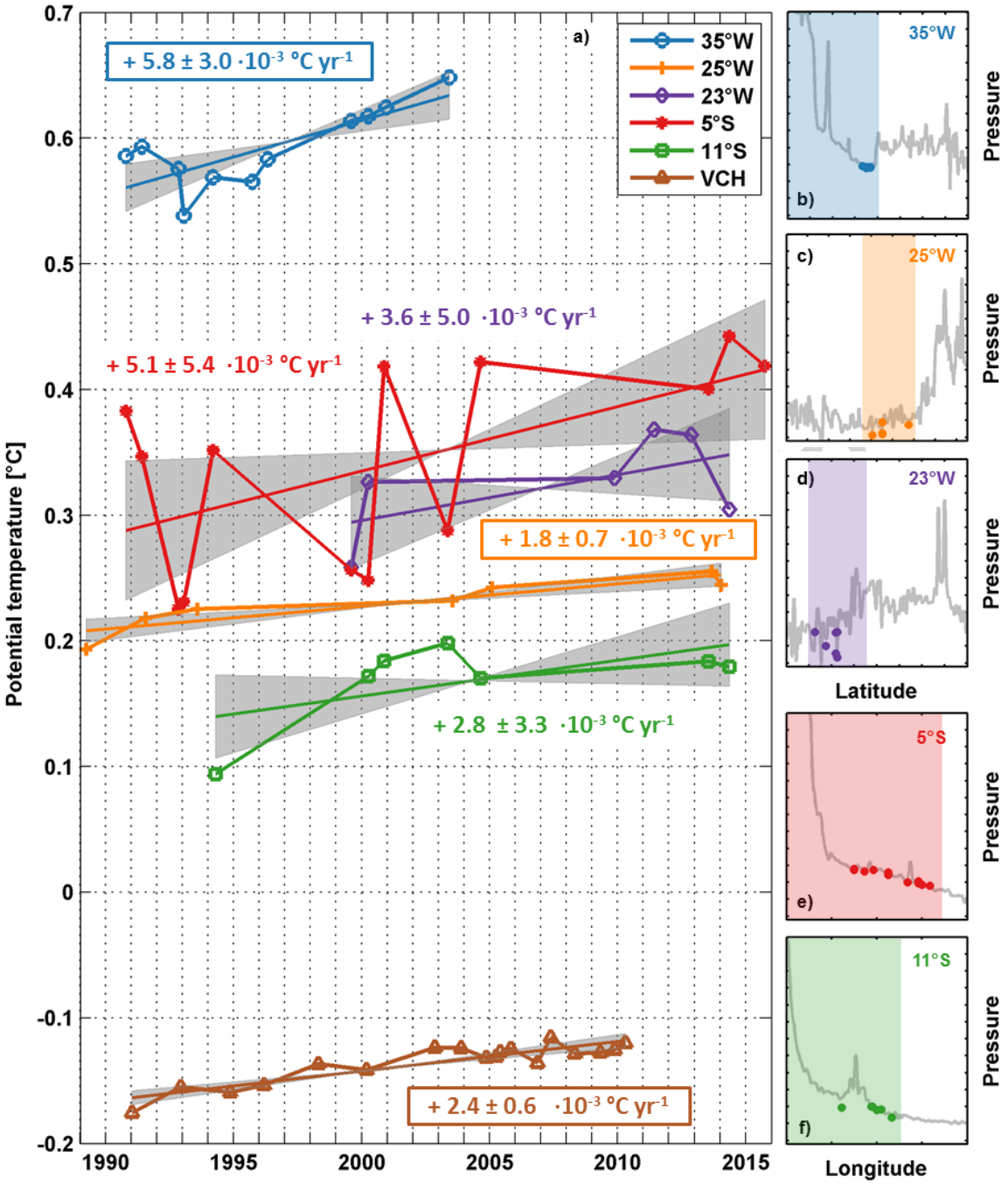

Figure 11 a) Evolution of θ [°C] of the coldest AABW found along the sections 35°W, 25°W, 23°W, 5°S, 11°S and within the Vema Channel (VCH). Linear fits are shown as solid lines, the colored numbers are the slopes of those linear fits (linear trends) in $\cdot 10^{-3}$ °C yr^{-1}. Also included are 95% confidence estimates (the standard error of the slope multiplied by 1.96), indicated by the grey shading. Boxes around the numbers highlight the trends different from zero at 95% confidence. b-f) Pressure contours (in the interval 0 - 6000 dbar) deduced from ETOPO1 are plotted together with colored dots, indicating where the lowest temperatures were measured within the individual sections. Colored shading indicates the section portion of this analysis.

Using neutral density as the vertical axis allows us to directly relate this prominent warming in the tropical Atlantic to a deepening of the isopycnals of the dense AABW. While the fraction of temperature change on isopycnals representing the dense AABW is rather small (between -0.5 and 0.7 $\cdot 10^{-3}$ °C yr^{-1}) and even changes sign depending on the period under consideration (Figure 12e,f), isopycnal surfaces themselves are shifted towards higher pressures everywhere in the entire denser AABW density range (Figure 12h,i). The downward displacement is most pronounced for $\gamma^n > 28.225$ kg m^{-3} where the positive trends in pressure tend to increase with depth (with 6.2 ± 3.5 dbar yr^{-1} on average, and reaching a maximum of 13.4 ± 4.2 dbar yr^{-1} in the northern Brazil Basin). The deepening of isopycnals of the dense AABW is different from zero when adding a 95% confidence estimate only for the whole time series but seems to become stronger during the 2000s. This result is an indication that the observed warming at those depths may be caused by a volume loss of the denser AABW layer during the period 1990 – 2014, which is in agreement with previous studies (e.g., Purkey and Johnson, 2013; Johnson et al., 2014).

b) Temperature changes in the lNADW/lighter AABW layers

Above 4500 dbar, the lighter AABW and the lNADW layers together show stronger θ changes which create a more complex picture as they differ according to location and period (Figure 12). In the EQCH, the lighter AABW shows a pronounced warming on isobars of about 5 – 10 $\cdot 10^{-3}$ °C yr^{-1} over the period 1990 – 2003, while the lNADW rather cools at a rate of -2 to -3 $\cdot 10^{-3}$ °C yr^{-1}. When comparing trends on corresponding isopycnals (28.135 – 28.225 kg m^{-3}), we find intrinsic warming in fact to be relatively strong in the lighter AABW layer (2.1 ± 1.6 $\cdot 10^{-3}$ °C yr^{-1}) whereby isopycnal heave stills has a dominant effect on changes on isobars in the EQCH. The deepening of isopycnals observed for the denser AABW layers in the basin interior seems to extend into the lighter AABW layer, albeit somewhat weaker (< 2 dbar yr^{-1}), while the isopycnals of the lNADW layer rise at maximum rates of -5.3 ± 2.1 dbar yr^{-1} which explains the observed negative trend on isobars (Figure 12d). In the northern Brazil Basin, the lNADW and lighter AABW layers show similar behavior over time, supporting our assumption that both water masses form a highly interactive transition layer in this region. However, we find intrinsic water mass changes to be the dominant process – exhibiting a two period behavior (Figure 12e). Both layers show intrinsic warming (1.6 ± 1.7 $\cdot 10^{-3}$ °C yr^{-1}) in the 1990s while also including the 2000s results in a net intrinsic cooling (-0.7 ± 0.6 $\cdot 10^{-3}$ °C yr^{-1}). While the intrinsic warming in the 1990s is almost homogeneously distributed, trends over the whole time series reverse sign on the densest isopycnals. However, the weak warming trend in the denser AABW layer for the whole time series corresponds - in combination with the strong warming in the 1990s – to a cooling in the 2000s. As in the EQCH, we observe that the deepening of isopycnals extends from the denser into the lighter AABW for $\gamma^n > 28.17$ kg m^{-3}, but no such trend is observed for both periods under consideration within all lighter layers. This

means that trends on isobars in the northern Brazil Basin above 4200 dbar are exclusively caused by changes in the spiciness of those layers.

In the VCH, isopycnals are generally found at lower pressures compared to the northern Brazil Basin. This, together with the vertical trend distribution not aligning with the water mass boundaries, questions the validity of our choice of water mass definitions in the VCH (see chapter 3 for a more detailed discussion). Based on the vertical trend distribution on isobars (Figure 12c) we would suggest a separation of the lighter from the denser AABW component in the VCH at about 4400 dbar, which corresponds to the γ^n = 28.25 kg m^{-3} isopycnal. Below this pressure we find the weak but uniformly distributed warming described before, 3.6 ± 2.1 ·10-3 °C yr^{-1} for 1989-2003 and 2.4 ± 1.1 ·10-3 °C yr^{-1} for 1989-2014.

Above the γ^n = 28.25 kg m^{-3} isopycnal we find stronger temperature changes with a pronounced vertical structure, although none of them are different from zero when at the 95% confidence limit: Temperature trends on isobars within the light AABW and lNADW layers follow an S-shaped curve with strong warming (up to 12.5 $\cdot 10^{-3}$ °C yr^{-1}) centered around 4100 dbar, and weak cooling (about -1.5 $\cdot 10^{-3}$ °C yr^{-1}) above 3700 dbar (Figure 12c). This shape is preserved over both periods under consideration (but partly shifted by more than -10 $\cdot 10^{-3}$ °C yr^{-1} towards negative trends for the 1990s) and actually reflects the effect of the displacement of isopycnals. It shows a thickening layer above and thinning layer below 28.18 kg m^{-3} in the 1990s. Considering the entire period 1990 – 2010 reveals a deepening of isopycnals extending over the whole density range of lNADW and AABW (being almost zero above 28.135 kg m^{-3}) which means that those layers also start to subside during the 2000s. Temperature changes on isopycnals are around zero below the 28.22 kg m^{-3} isopycnal and show a vertical structure with zero crossings above but the slope errors are very large. In the VCH, temperature anomalies on isopycnals, used to fit the linear trends, generally vary over a broader range.

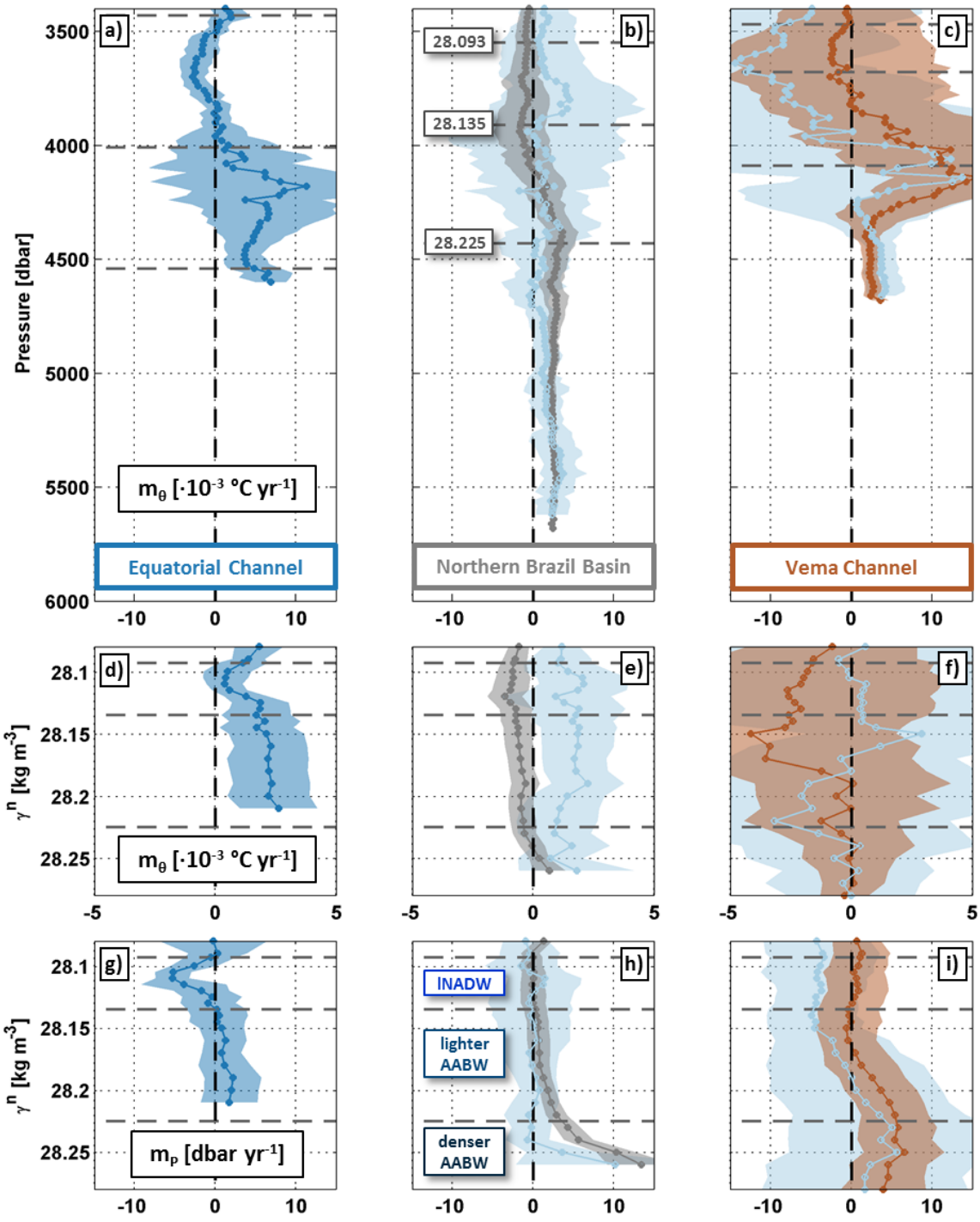

Figure 12 Linear trends (= slopes of the linear fits to weighted anomalies) of potential temperature m_θ [$\cdot 10^{-3}$ °C yr^{-1}] on pressure levels (a-c) and on isopycnals (d-f), as well as of pressure m_p [dbar yr^{-1}] of the corresponding isopycnals (g-i). The trends are shown for the lNADW and AABW layers, grey dashed lines mark the isopycnal water mass boundaries γ^n [kg m^{-3}] or their average pressures. Color coding distinguishes between different regions and periods: darker blue for trends within the EQCH (along 35°W, south of 1°N) over the period 1990 – 2003; grey for trends within the northern Brazil Basin, the time series combining relevant measurements along 11°S, 5°S, 25°W and 23°W over the period 1989 – 2014; brown for trends within the VCH over the period 1990 – 2010; light blue for 1990 – 2003 subsets of the two longer time series. Transparent shading gives a 95% confidence interval estimate (the standard error of the slope multiplied by 1.96).

c) Evolution of bottom neutral density in the EQCH

The γ^n = 28.225 kg m^{-3} isopycnal, which separates the lighter from the denser AABW in the northern Brazil Basin, is apparent in the EQCH only in 1993. Before 1993 bottom density in the deepest parts of the EQCH gradually increased. The isopycnals spanning the lighter AABW layer rose from 1991 to 1993, but deepened afterwards together with the isopycnals above. The disappearance of the isopycnals 28.22 kg m^{-3} < γ^n < 28.225 kg m^{-3} on the equator, which typically coincide with the 0.6 °C isotherm there, was reported by earlier studies. For example, Limeburner et al. (2005) found water colder than 0.6 °C on the equator at 36°W in a 100 m thick bottom layer in 1992, being almost absent in 1994 and nonexistent in 1999, 2001, 2003. In addition, Rhein et al. (1995) found chlorofluoromethane (CFM) concentrations of AABW at 35°W and 5°S to be near the detection limit in October 1990 and early summer 1991, but slightly increased in June 1991 at 5°S and in November 1992 at 35°W. They interpreted this as the arrival of "young" WSDW components (F11 concentration > 0.015 pmol kg^{-1}) in the early 1990s. The dataset analyzed here includes measurements along the 10°S and 31°W sections which were measured only in 1992 and 1994. Along these sections we additionally find temperatures on the γ^n = 28.25 kg m^{-3} isopycnal (within the core of the denser AABW; Figure 6d) to be noticeably lower compared to long-term averages along the repeated sections. Such cold anomalies on isopycnals within the dense AABW support the arrival of even colder AABW at the equator in the early 1990s.

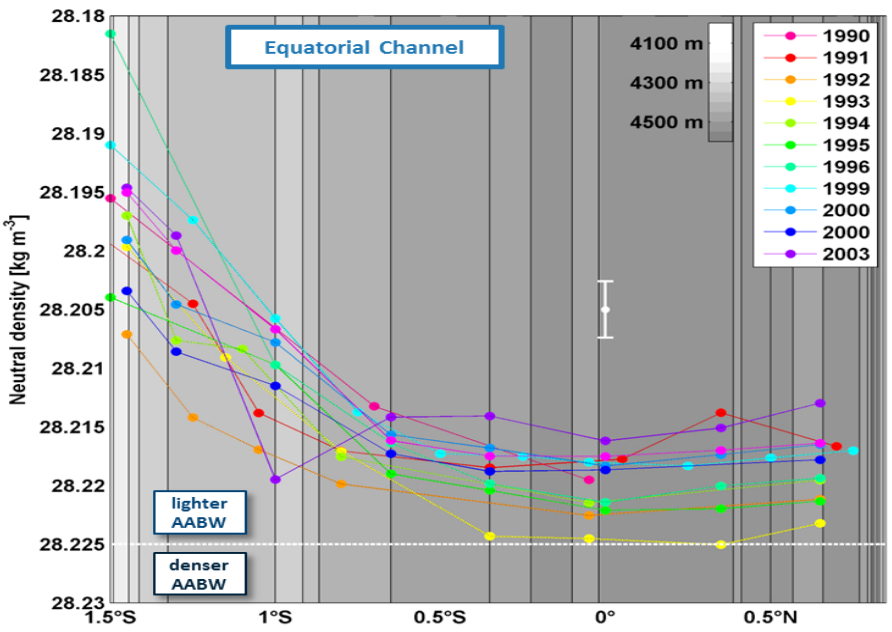

Figure 13 The evolution of bottom neutral density [kg m^{-3}] in the EQCH over the period 1990-2003. Grey shading represents ETOPO1 bathymetry (with contour intervals of 50 m). The white dashed line denotes the lighter/denser AABW boundary. The white errrorbar gives the maximum error range in the

local neutral density (for the EQCH region and 28.18 kg m^{-3} < γ^n < 28.23 kg m^{-3}) arising from the inaccuracy in θ and S measurements.

6. SUMMARY AND CONCLUSIONS

In this study, CTD and LADCP data from repeated ship sections in the western equatorial Atlantic (along 35°W, 25°W, 23°W, 5°S and 11°S) and in the VCH (Figure 2), all together spanning the period 1989 – 2014, are analyzed regarding the spatial and temporal property changes of mNADW, lNADW and AABW. In terms of water masses, pathways and along-pathway transformation, we discuss the results of our analysis mainly with respect to previous results, thus substantiating the earlier findings that were obtained with reduced datasets and coverage. Finally, we present the observed long-term changes of the different analyzed water masses, taking into account the full length of the time series at different locations to update the earlier results.

a) Deep and bottom waters entering the Brazil Basin from the North and South

The mNADW and lNADW layers entering the Brazil Basin through the EQCH are characterized by high oxygen levels reaching down to about 4000 dbar (Figure 3b), and relatively high temperatures on core isopycnals (Figure 6a,b). At 35°W, the mNADW and lNADW flow is concentrated in a well-defined current core topographically guided by the Parnaiba Ridge at 1.5°S, as reported by Rhein et al. (1995) and Schott et al. (2003). Upon arrival in the northern Brazil Basin, the NADW characteristics are the result of strong modifications that occurred all along its way from the subpolar North Atlantic into the tropics (e.g., Arhan et al., 1998; Vanicek and Siedler, 2002; Demidov et al., 2003; Morozov et al., 2010). Upon their arrival at the equator after about 30 years, remaining fractions of LSW and DSOW within the DWBC are estimated to be below 15% of the original water masses (Rhein et al., 2015).

The AABW enters the Brazil Basin through the VCH with minimum temperatures of -0.18 °C (Figure 8c). The more isolated AABW is also known to mix with the overlying less dense water masses along its pathway from around Antarctica into the Brazil Basin. According to Coles et al. (1996), this is a simple two end-member process in which the WSDW mainly mixes with the LCPW in the Argentine and southern Brazil Basin. Low oxygen concentrations found within all AABW layers in the investigated region confirm LCPW dominance in the Brazil Basin, as proposed by Mantyla and Reid (1983), Reid (1989), Sandoval and Weatherly (2001), or in a water mass analysis for the South Atlantic presented by Demidov et al. (2012).

b) Mean pathways and spatial property changes within the northern Brazil Basin

Shortly after crossing the equator, the NADW separates into different branches with different representation in the individual NADW layers (Rhein et al., 1995; 1998; Larque et al., 1997; Richardson and Fratantoni, 1999; Schott et al., 2005). Our dataset allows us to investigate the two major routes for the mNADW and lNADW in the northern Brazil: the southward flow of the DWBC and the eastward flow slightly south of the equator.

While the warm signature of the mNADW layer can be clearly traced together with the velocity signal of the DWBC southward along the continental slope (Figure 6a), the transport of lNADW drastically decreases from the 35°W section to the 5°S section (Figure 6b), as was previously reported by Friedrichs et al. (1994) and Schott et al. (2005). Farther south the separation between mNADW and lNADW becomes less clear as their contributions change (e.g., Figure 5a,b), indicating that both water masses are strongly transformed on their way along the western boundary. The strongest modifications apparently occur around 4 – 5°S (Figures 6 or 10) where the Ceará Seamount Chain may be responsible for enhanced mixing. The shear between intensified western boundary currents in the NADW and AABW of opposite direction could also contribute to enhanced mixing along this pathway – with the combined effects may be sufficient to dilute the lNADW characteristics in the southward flow of the remaining lNADW within the DWBC. Additionally, we find indications for a different water mass coming from the Southeast to fill the mNADW density range away from the western boundary (Figures 9a, 10a) and possibly joining the DWBC somewhere between 4 – 6°S. The corresponding θ distribution (Figure 6a) matches best the pathways of mNADW proposed by Friedrichs et al. (1994) who assumed that this other water mass was modified or recirculated water coming from the western boundary or the southern Brazil Basin. More recently in a water mass analysis for the South Atlantic, Demidov et al. (2012) suggested that mNADW may penetrate from the East Atlantic into the western basin somewhere south of 20°N. Aside from the southward DWBC, several studies reported another, equally preferred route for the NADW layers eastward along the equator (e.g., Weiss et al., 1985; Richardson and Fratantoni, 1999; Gouriou et al., 2001; Rhein et al., 2015). In agreement with these studies, we are able to follow the pronounced O_2 maximum in the lNADW and mNADW layers in a confined band at 2 – 3°S parallel to the equator (Figure 3b,d) and even can locate it at the entrances to RCHFZ (Figure 4b), coinciding with an eastward current band extending over all deep layers along 23°W (Figure 6d). This eastward extension of the NADW flow may in part also explain the disappearance of large lNADW fractions off Brazil. This path may be dynamically connected to the nearly barotropic flow of the Equatorial Intermediate Current System, with eastward flow at about 2°S and 2°N and westward flow in between (for a mean 23°W section of zonal velocity, see Greatbatch et al. (2012)). Ascani et al. (2010, 2015) found such current bands in idealized model simulations without any MOC. In these model results the eastward current bands at 2°S and 2°N, which originate close to the western boundary and reach down to the bottom, are

generated by the rectification of downward propagating intra-seasonal waves. The interaction of such flow with the AMOC in a more realistic setting would be of great relevance for the understanding of deep and bottom water mass pathways.

Below 4000 – 4500 dbar, linearly decreasing salinity, potential temperature and dissolved oxygen indicate the presence of AABW in the northern Brazil Basin (Figure 8). We separate a lighter from a denser AABW in the northern Brazil Basin by the γ^n = 28.225 kg m^{-3} isopycnal, since we observe different spatial and temporal behavior for the layers above and below (Figure 12). In the tropical Atlantic, this isopycnal typically coincides with the 0.6 °C isotherm. Water colder than 0.2 °C can only be found along 11°S where the measured section covers the interior of the deep Brazil Basin (Figure 5c) while temperatures measured in the EQCH are always above 0.55 °C (Figure 3a). The northward transport of AABW is partly confined along the western boundary just below the DWBC (Figure 6c), transporting the lighter version of AABW and probably feeding the flow of AABW into the North Atlantic via the EQCH. The denser AABW layers, at larger amounts than the lighter AABW, are transported northward in the interior of the basin at levels deeper than 4500-4700 dbar (Figure 6d). The flow of denser AABW is assumed to turn east at about 5°S following the topography parallel to the equator towards the RCHFZs (e.g., Sandoval and Weatherly, 2001).

In the entire northern Brazil Basin we find that the lNADW and the lighter AABW together form a highly interactive transition layer above 4500 dbar. Their temperature distributions on isopycnals (Figures 6b,c) gradually change as both water masses experience mixing along their pathways. The strongest mixing occurs along the western boundary where the AABW becomes more saline and warms, and the lNADW freshens and cools by an equal amount (Figure 8b,c). At the same time the AABW loses its densest end-member which is in agreement with several previous studies (e.g., Reid, 1989, Sandoval and Weatherly, 2001). Away from the western boundary, temperature distributions on isopycnals within the lNADW and lighter AABW (Figure 8b,c) reveal a pattern in which the lower temperatures of AABW dominate the entire density range in the central to eastern interior parts of the Brazil Basin. North of 5°S, the warmer temperatures indicate the dominance of lNADW. Along the eastward pathway parallel to the equator (Figure 9) we find AABW to be more homogenized and a much weaker freshening of the lNADW. Less pronounced property changes along this route could be due to the rather smooth topography. In fact, the AABW - already strongly transformed north of 5°S and flowing into the same direction as the lNADW - diminishes its vertical shear.

c) Long-term temperature changes

As our dataset from the northern Brazil Basin spans 26 years with up to 50 realizations, it can be treated as a multi-decadal time series. In accordance with previous studies focusing on the VCH (e.g., Zenk and

Morozov, 2007; Zenk and Visbeck, 2013), we investigate the evolution of the lowest temperatures found along each of the five sections 35°W, 25°W, 23°W, 5°S, 11°S (Figure 11). The calculated trends at 11°S ($+2.8 \pm 3.3 \cdot 10^{-3}$ °C yr^{-1} for the period 1994 – 2014), 25°W ($+1.8 \pm 0.7 \cdot 10^{-3}$ °C yr^{-1} for the period 1989 – 2014) and 23°W ($+3.6 \pm 5.0 \cdot 10^{-3}$ °C yr^{-1} for the period 1999 – 2014), where we mainly capture denser AABW, are similar to those found in the VCH. But trends are up to two times larger at 5°S ($+5.1 \pm 5.4 \cdot 10^{-3}$ °C yr^{-1} for the period 1990 – 2014) and 35°W ($+5.8 \pm 3.0 \cdot 10^{-3}$ °C yr^{-1} for the period 1990 – 2003) where lighter AABW component dominates. The large temperature changes at the bottom of the EQCH, the warming trends at 25°W from 1989 – 2014 and in the VCH from 1990 – 2010, are the only ones different from zero when adding a 95% confidence limit. When combining local results into one time series for a larger, dynamically connected region – the northern Brazil Basin (Figure 12b), we are able to derive a warming of the densest AABW component of about $2.5 \pm 0.7 \cdot 10^{-3}$ °C yr^{-1} throughout the period 1989 – 2014, which is different from zero when adding a 95% confidence limit over different periods and almost uniformly distributed in the relevant pressure range. Also in the Brazil Basin, for example, Johnson and Doney (2006) found a small but statistically significant (different from zero at 95% confidence limits) warming of about $2.4 – 4.4 \cdot 10^{-3}$ °C yr^{1} (0.04 °C from 1989/1995 to 2003/2005) on isobars in the most homogenous abyssal waters deeper than 4500 dbar. More recently, Johnson et al. (2014) reported a warming trend of up to $2 – 3 \cdot 10^{-3}$ °C yr^{-1} from 1989 to 2014 at pressures greater than 4300 dbar which is also statistically significant. Changes on isobaric surfaces can be decomposed into changes on isopycnal surfaces and the vertical displacement of those surfaces. Using neutral density as the vertical axis allows us to directly relate the warming in the tropical Atlantic to a volume loss of the denser AABW as the corresponding isopycnal surfaces are shifted towards higher pressure levels everywhere in the entire AABW density range (Figure 12h). The downward displacement is most pronounced for the $\gamma^n > 28.225$ kg m^{-3} isoycnals where the positive trends in pressure increase with depth (6.2 ± 3.5 dbar yr^{-1} on average; 13.4 ± 4.2 dbar yr^{-1} maximum). This result is an indication for the observed warming at those depths to be mainly caused by a downward displacement of the isopycnals corresponding to a loss of volume of the denser AABW component during the period 1990 – 2014. The volume loss in the tropical Atlantic appears to be consistent with findings by Purkey and Johnson (2012) who observed a decrease in volume of 8 Sv of the coldest and deepest waters throughout the entire Southern Ocean from 1980 to 2010 which is equivalent to a descent of the 0 °C potential isotherm of about 10 dbar yr^{-1}. Similarly for the Brazil Basin, Johnson et al. (2014) found a decrease of the vertical extent of waters with $\theta < 0.25$ °C during the period 1989 – 2014, where isotherms descend at depth-increasing rates - up to a maximum rate of about 11 dbar yr^{-1} at $\theta = 0.25$°C.

The transition layer formed by the lNADW and lighter AABW components in the western tropical Atlantic shows stronger, but also incoherent θ changes. In the EQCH and VCH, we found isopycnal heave

to still have the dominant effect on the vertical distribution of θ trends on isobars (Figures 12g,i), reflecting the contraction of the AABW layers below and expansion of the NADW layers above. For the entire Brazil Basin, Johnson et al. (2014) observed the layer thickness of waters with $0.25 < \theta < 1.2$ °C to increase as the $1.2 < \theta < 2$ °C isotherms rise at a maximum rate of -1.5 dbar yr^{-1}. They found the contraction of the densest waters and expansion of lighter waters over the last 25 years was accompanied by a shift among waters from one temperature class to another. However, we also find relatively strong θ changes on isopycnals at all locations (Figure 12d, e,f). In both layers, temperatures on isopycnals exhibit decadal variations with warming in the 1990s and cooling in the 2000s. The contributions to the trends on isobars range from about 50% in the lighter AABW layers in the EQCH to up to 80% within the lNADW/lighter AABW layers in the northern Brazil Basin. The cooling on isopycnals in the 2000s was also reported by Hummels et al. (2015) for the 5°S and 11°S sections to extend over all NADW layers and associated with increasing oxygen.

Reversing changes were also found for the bottom density in the EQCH (Figure 13). While the density in the deepest part of the channel increased from 1990 to a maximum in 1993, it decreased afterward to reach its lowest values in 2003 (which corresponds to the time of the last available measurements at this location). The decrease in bottom density represents a deepening of the isopycnals in the lighter AABW layer (Figure 12g). Limeburner et al. (2005) found water colder than 0.6 °C on the equator at 36°W in a 100 m thick bottom layer in 1992, being almost absent in 1994 and nonexistent in 1999, 2001, 2003. In addition, Rhein et al. (1995) found chlorofluoromethane (CFM) concentrations of AABW at 35°W and 5°S to be near the detection limit in October 1990 and early summer 1991, but slightly increased in June 1991 at 5°S and in November 1992 at 35°W. Farther north at 24.5°N, Frajka-Williams et al. (2011) reported the layer of water colder than 1.5 °C to increase from zero in 1957 to a peak in 1992 before decreasing monotonically through the years 1998, 2004 and near zero in 2010. However, at warmer isotherms they found a different temporal evolution. When including water between 1.5 – 1.8 °C in the AABW definition, the years 1998, 2004 and 2010 showed the thickest layer of water. This indicates a decrease in the volume of the coldest waters at that location but also a shift to slightly warmer temperatures in the lighter AABW components during those specific years. The abyssal northward flow across 24°N decreased between 1981 and 2010 but also shows a recent rebound from a minimum in 2004 (Frajka-Williams et al., 2011).

The causes for the globally occurring warming signal in the AABW are manifold and still under investigation. Some studies suggested a reduction of AABW formation associated with a slowdown of the bottom limb of the MOC as a possible explanation (e.g., Johnson et al., 2008; Purkey and Johnson, 2012). A slower production rate would cause isopycnals to descend, observable as a warming on isobars, but also contribute to warming on isopycnals as slower spreading allows for an extended period of mixing with

surrounding waters. Some studies attempted to directly relate the observed warming in the subtropical and tropical Atlantic to an abyssal warming in the Weddell Sea, being a potential thermal recovery subsequent to the Weddell Polynya closing in the 1970s (e.g., Coles et al., 1996; Robertson et al., 2002; Johnson et al., 2014). Alternative hypotheses relate the warming of abyssal waters in the Atlantic Ocean to a strengthening of westerly winds around Antarctica, restricting the export of bottom waters from the Weddell Gyre (e.g., Fahrbach et al., 2011). Additionally, the southward migration of westerlies was found to result in a net increase of NADW inflow into the South Atlantic and an increase in the northward Ekman transport, probably leading to a strengthening of CDW upwelling (e.g., Oke and England, 2004). It can be argued that reduced Antarctic Shelf Water production or enhanced CDW/WDW contributions to AABW formation would affect AABW properties in the way that the same amount but a lighter version of AABW is produced (e.g., Shimada et al., 2012; Azaneu et al., 2013; van Wijk and Rintoul, 2014).

Regardless of its cause, there is also the question of how the AABW warming signal progresses into the South and equatorial Atlantic: In the Southern Ocean it is assumed that the pattern of abyssal warming is at least partly caused by advection of warmer water with the mean abyssal flow field (e.g., Patara and Böning, 2014). Outside of the Southern Ocean, however, the rapid northward propagation of this signal, for example manifested in the onset of the warming trend in the VCH starting in 1992, cannot be explained by the weak abyssal circulation alone as ventilation in the bottom overturning cell happens on centennial timescales. Adjustment due to vertical displacement of deep isopycnals, on the other hand, is a signal that can be communicated by boundary waves throughout the oceans on much shorter time scales (years to decades) than by the advective transport of water mass anomalies (e.g., Swingedouw et al., 2009; Masuda et al., 2010; Purkey and Johnson, 2012).

Following Johnson et al. (2014), a warming in the deep waters of the Weddell Sea after the disappearance of the mid-1970s Weddell Polynya could reduce the amount of the dense waters (or their warming) exported into the western Atlantic. This would cause heave-induced warming in the abyssal waters of the Argentine Basin from the 1970s through about 2005, followed by a warming in the VCH since 1992, and a subsequent warming in the Brazil Basin within the period 1989 – 2014, and its arrival at the equator no later than 1994. The trends presented in this study for the northern Brazil Basin support the notion that the warming in the densest AABW is mainly caused by a downward displacement of isopycnals, and subsequently communicated by boundary waves as this signal reaches the equator in the mid-1990s.

Patara and Böning (2014) investigated the dynamical impact of abyssal warming around Antarctica on the AMOC with an ocean-sea ice model. They simulated a multi-decadal AABW warming trend of up to 5 $\cdot 10^{-3}$ °C yr^{-1}. The simulated warming signal entered the Atlantic basin after about 20 years from its onset, then rapidly propagated towards the equator within a few years – probably transmitted via Kelvin waves

along the western boundary and equator – and was then followed by a gradual northward progression into the North Atlantic within decades through the slower adjustment by Rossby waves generated at the eastern boundaries. Changing the vertical shear of meridional velocities, the propagating warming signal is accompanied by a weakening in the AABW transport of about 20% along 30°S, which is consistent with estimates based on observational data (Johnson et al., 2008). At the same time, Patara and Böning (2014) found the upper cell of the AMOC to rather strengthen and expand downward which would support a proposed "seesaw" behavior between the NADW and AABW cells on decadal to centennial timescales (e.g., Swingedouw et al., 2009; Martin et al., 2014). Although long-term changes in the western boundary current transport off Brazil were found to be closely related to AMOC changes in numerical simulation (Rühs et al., 2015), those could not yet be identified in moored observations at 11°S from 2000-2004 and 2013-2014 (Hummels et al., 2015). Calculating a 50-year geostrophic transport time series for the North Brazil Current, Zhang et al. (2011) found strong multi-decadal variability without any significant trend.

However, we also observe substantial decadal temperature changes on isopycnal surfaces in the northern Brazil Basin - with warming in 1990s and cooling in the 2000s. Being intrinsic changes, those have to be transported into the western tropical Atlantic via slow advection. Whether this signal is due to variability of water mass formation in the Southern Ocean or North Atlantic, or associated with varying lateral and vertical mixing processes along the transport pathways, remains an open question. Particularly along the deep western boundary route, vertical mixing might change due to the concurrent vertical displacements of isopycnal surfaces. Vertical mixing has the potential to contribute to variability on interannual to decadal time scales. Changing characteristics of newly formed water masses, which might be diluted along the pathway toward the northern Brazil Basin, could contribute to the variability on multi-decadal time scales.

The deep ocean is an integral part of the climate system and is known to transport large amounts of heat. Therefore, changes in the water mass properties of NADW and AABW, especially on longer timescales, are of particular interest. Up to now, it remains an unresolved issue if the observed changes of deep and bottom waters are associated with climate change or long-term ocean and climate variability. Sustained observations are needed, as well as the development of an observing system which allows for a better monitoring of these changes – either by better exploiting existing shipboard and moored observation or by conceiving and applying new techniques, such as gliders and deep Argo floats (see e.g., Deep Argo Implementation Workshop at http://www.argo.ucsd.edu/DAIW1report.pdf). As field measurements tend to be limited in space and time, adequate high-resolution models should be analyzed in parallel regarding the temporal variability of abyssal waters.

Acknowledgements

This study was funded by the Deutsche Bundesministerium fu□r Bildung und Forschung (BMBF) as part of the project RACE (03F0651B) and through support of R/V Sonne cruises, as well as by the Deutsche Forschungsgemeinschaft through cruises with R/V Meteor and R/V Maria S. Merian. We greatly appreciate the careful and sustained work of the officers, crew, and scientific parties involved in many scientific programs contributing to collect deep CTD and velocity data in the tropical and South Atlantic. Further, we would like to thank S.-H. Didwischus, R. Hummels and G. Krahmann for providing us with the well-sorted data, S. Schmidtko and K. Getzlaff for significantly improving this work with their comments, and R. Zantopp for proofreading. We truly appreciate comprehensive and constructive suggestions from the five anonymous reviewers.

References

Amante C and Eakins BW (2009). ETOPO1 1 Arc-Minute Global Relief Model: Procedures, Data Sources and Analysis. NOAA Technical Memorandum NESDIS NGDC-24. National Geophysical Data Center, NOAA. doi:10.7289/ V5C8276M [26/03/14].

Andrie C, Gouriou Y, Bourles B, Ternon JF, Braga ES, Morin P and Oudot C (2003). Variability of AABW properties in the equatorial channel at 35°W. *Geophys Res Lett*, 30(5), 8007.

Arhan M, Mercier H, Bourles B and Gouriou Y (1998). Hydrographic sections across the Atlantic at 7°30 ' N and 4°30 ' S. *Deep-Sea Res I*, 45, 829-872.

Ascani F, Firing E, Dutrieux P, McCreary JP and Ishida A (2010). Deep equatorial ocean circulation induced by a forced-dissipated Yanai beam. *J Phys Oceanogr*, 40, 1118-1142.

Ascani F, Firing E, McCreary JP, Brandt P and Greatbatch RJ (2015). The deep equatorial ocean circulation in wind-forced numerical solutions. *J Phys Oceanogr*, 45 (6), 1709-1734. doi:10.1175/JPO-D-14-0171.1.

Azaneu M, Kerr R, Mata MM and Garcia CAE (2013). Trends in the deep Southern Ocean (1958–2010): Implications for Antarctic Bottom Water properties and volume export. *J Geophys Res Oceans*, 118, 4213–4227, doi:10.1002/jgrc.20303.

Bindoff NL and McDougall TJ (1994). Diagnosing Climate Change and Ocean Ventilation Using Hydrographic Data. *J Phys Oceanogr*, 24, 1137-1152.

Bower AS, Lozier MS, Gary SF and Böning CW (2009). Interior pathways of the North Atlantic meridional overturning circulation. *Nature*, 459, 243-247.

Coles VJ, McCartney MS, Olson DB and Smethie WM Jr (1996). Changes in Antarctic Bottom Water properties in the western South Atlantic in the late 1980s. *J Geophys Res*, 101, 8957–8970.

Couldrey MP, Jullion L, Naveira Garabato AC, Rye C, Herraiz-Borreguero L,Brown PJ, Meredith MP and Speer KL (2013). Remotely induced warming of Antarctic Bottom Water in the eastern Weddell gyre. *Geophys Res Lett*, 40, 2755-2760. doi:10.1002/grl.50526.

Demidov AN (2003). Distinguishing the intermediate and deep water masses in the South Atlantic, *Oceanology*, 43, 153-163.

Demidov AN, Dobrolyubov SA, Morozov EG and Tarakanov RY (2007). Transport of bottom waters through the Vema Fracture Zone in the Mid-Atlantic ridge. *Doklady Akademii Nauk*, 416 (3), pp. 395–399.

Demidov, AN, Krayushkin, EV, Kalashnikov,a NA and Chereshnuk, SA (2012).Water mass structure in the South Atlantic and its decadal variability. Presented at the International Climate Change Symposium, May 13-20, 2012, Yeosu, Korea. Retrieved from http://www.pices.int/publications/ presentations/2012-Climate-Change/S1/Day2-1500-Demidov-S1.pdf [25/09/15].

Dengler M, Schott FA, Eden C, Brandt P, Fischer J and Zantopp RJ (2004). Break-up of the Atlantic deep western boundary into eddies at 8°S. *Nature*, 432, 1018-1020.

Dickson RR and Brown J (1994). The production of North Atlantic Deep Water: Sources, rates, and pathways, *J Geophys Res*, 99(C6), 12319–12342.

Durack PJ and Wijffels SE (2010). Fifty-Year Trends in Global Ocean Salinities and Their Relationship to Broad-Scale Warming. *J Climate*, 23, 4342–4362. doi: http://dx.doi.org/10.1175/2010JCLI3377.1

Emery WJ and Thompson RE (2004). Data Analysis Methods in Physical Oceanography, 2nd ed., Elsevier, San Diego, Calif.

Fahrbach, E, Hoppema, M, Rohardt, G, Schröder, M, Wisotzki, A (2004). Decadal-scale variations of water mass properties in the deep Weddell Sea. *Ocean Dyn*, 54, 77–91.

Fahrbach E, Hoppema M, Rohardt G, Boebel O, Klatt O and Wisotzki A (2011). Warming of deep and abyssal water masses along the Greenwich meridian on decadal timescales: The Weddell gyre as a heat buffer. *Deep-Sea Res II*, 58, 2509-2523.

Fischer J and Visbeck M (1993). Deep velocity profiling with self-contained ADCPs. *J Atmos and Oceanic Tech*, 10, 764–773.

Frajka-Williams E, Cunningham SA, Bryden H and. King BA (2011). Variability of Antarctic Bottom Water at 24.5ºN in the Atlantic. *J Geophys Res*, 116, C11026.

Friedrichs, MAM, McCartney MS, and Hall MM (1994). Hemispheric asymmetry of deep water transport modes in the western Atlantic. *J Geophys Res*, 99(C12), 25165–25179.

Fukasawa M, Freeland H, Perkin R, Watanabe T, Uchida H and Nishina A (2004). Bottom water warming in the North Pacific Ocean. *Nature*, 427, 825–827.

Ganachaud, A (2003). Large-scale mass transports, water mass formation, and diffusivities estimated from World Ocean Circulation Experiment (WOCE) hydrographic data. *J Geophys Res*, 108, 3213, doi:10.1029/2002JC001565, C7.

Garzoli LS, Dong S, Fine R, Meinen C, Perez RC, Schmid C, van Sebille E and Yao Q (2015). The fate of the Deep Western Boundary Current in the South Atlantic. *Deep-Sea Res*, 103, 125-136. doi:10.1016/j.dsr.2015.05.008.

Gouriou Y., et al. (2001). Deep circulation in the equatorial Atlantic Ocean, *Geophys Res Lett*, 28, 819–822.

Greatbatch RJ, Brandt P, Claus M, Didwischus SH, and Fu Y (2012). On the width of the equatorial deep jets. *J Phys Oceanogr*, 42, 1729–1740. doi:10.1175/JPO-D-11-0238.1.

Hall MM, McCartney MS and Whitehead JA (1997). Antarctic Bottom Water flux in the Equatorial Western Atlantic. *J Phys Oceanogr*, 27(9), 1903-1926.

Hogg N, Siedler G, Zenk W (1999). Circulation and variability at the southern boundary of the Brazil Basin. *J Phys Oceanogr* 29:145-157.

Hogg NG and Owens WB (1999). Direct measurement of the deep circulation within the Brazil Basin. *Deep-Sea Res II*, 46, 335–353.

Hogg NG and Thurnherr M (2005) A zonal pathway for NADW in the South Atlantic. *J Oceanogr*, 61, 493-507.

Hummels R, Brandt P, Dengler M, Fischer J, Araujo M, Veleda D and Durgadoo JV (2015), Interannual to decadal changes in the western boundary circulation in the Atlantic at 11°S, *Geophys Res Lett*, 42, doi:10.1002/ 2015GL065254.

Jackett DR and McDougall TJ (1997). A Neutral Density Variable for the World's Oceans. *J Phys Oceanogr*, 27, 237–263.

Johnson GC and. Doney SC (2006). Recent western South Atlantic bottom water warming, *Geophys Res Lett*, 33, L1461.

Johnson, GC, Purkey SG, and Toole JM (2008). Reduced Antarctic meridional overturning circulation reaches the North Atlantic Ocean. *Geophys Res Lett*, 35, L22601, doi:10.1029/2008GL035619.

Johnson, GC, McTaggart KE and Wanninkhof R (2014). Antarctic Bottom Water temperature changes in the western South Atlantic from 1989 to 2014. *J Geophys Res Oceans*, 119, 8567–8577, doi:10.1002/2014JC010367.

Kieke D and Yashayaev I (2015). Studies of Labrador Sea Water formation and variability in the subpolar North Atlantic in the light of international partnership and collaboration. *Prog Oceanogr*, 132(3), 220-232, doi:10.1016/j.pocean.2014.12.010.

Larque L, Maamaatuaiahutapu K and Garcon V (1997). On the intermediate and deep water flows in the South Atlantic Ocean. *J Geophys Res Oceans,*. 102 (C6), 12425-12440.

Limeburner R, Whitehead JA and Cenedese C (2005). Variability of Antarctic Bottom Water flow into the North Atlantic. *Deep-Sea Res II*, 52, 495-412.

Lumpkin R and Speer K. (2007). Global Ocean Meridional Overturning. *J Phys Oceanogr*, **37**, 2550–2562. doi: http://dx.doi.org/10.1175/JPO3130.1.

Lux M, Mercier H and Arhan M (2001). Interhemispheric exchanges of mass and heat in the Atlantic Ocean in January-March 1993. *Deep-Sea Res I*, 48, 605-638.

Mantyla AW and Reid JL (1983). Abyssal characteristics of the World Ocean waters. *Deep Sea Res*, 30(8), 805-833.

Masuda S, Awaji T, Sugiura N, Matthews JP, Toyoda T, Kawai Y, Doi T, Kouketsu S, Hiromichi Igarashi H, Katsumata K, Uchida H, Kawano T, Fukasawa M (2010). Simulated rapid warming of abyssal north pacific waters. *Science*, 329, 319–322.

Martin, T, Park W and Latif M (2014). Multi-Centennial Variability Controlled by Southern Ocean Convection in the Kiel Climate Model. *Climate Dynamics*, 40(7), 2005-2022, doi:10.1007/s00382-012-1586-7.

McCartney MS (1992). Recirculating components to the deep boundary current of the Northern North Atlantic. *Prog Oceanogr*, 29, 283-383.

Mercier H and Morin P (1997). Hydrography of the Romanche and Chain Fracture Zones. *J Geophys Res Oceans*, 102, 10373-10389.

Mercier H and Speer KG (1998). Transport of bottom water in the Romanche Fracture Zone and the Chain fracture zone. *J Phys Oceanogr*, 28(5), 779-790.

Messias MJ, Andrie C, Mèmery L and Mercier H (1999). Tracing the North Atlantic Deep Water through the Romanche and Chain fracture zones with chlorofluoromethanes. *Deep-Sea Res I*, 46, 1247-1278.

Morozov, E.G., Demidov, A.N., Tarakanov, R.Y. and Zenk, W. (2010). Abyssal Channels in the Atlantic Ocean: Water Structure and Flows. Editor: Georges Weatherly. *Berlin, Heidelberg*: Springer Science+Business Media B.V. Print.

Morris MY, Hall MM, St.Laurent LC and Hogg NG (2001). Abyssal Mixing in the Brazil Basin. *J Phys Oceanogr*, 31, 3331–3348.

Oke PR and England MH (2004). Oceanic response to changes in the latitude of the Southern Hemisphere subpolar westerly winds. *J Climate*, 17, 1040-1054.

Orsi AH Smethie WM and Bullister JL. (1999). Circulation, mixing, and production of Antarctic Bottom Water. *Prog Oceanogr*, 43, 55-109.

Patara L and Böning C (2014). Abyssal ocean warming around Antarctica strengthens the Atlantic overturning circulation. *Geophys Res Lett*, 41, 3972–3978.

Peterson RG and Whitworth III T (1989). The subantarctic and polar fronts in relation to deep water masses through the southwestern Atlantic. *J Geophys Res*, 94(C8), 10817–10838.

Pickart RS, Straneo F and Moore GWK (2003). Is Labrador Sea Water formed in the Irminger basin? *Deep-Sea Res I*. 50, 23-52.

Polzin KL, Toole JM, Ledwell JR and Schmitt RW (1997). Spatial variability of turbulent mixing in the abyssal ocean. *Science*, 276, 93-96.

Purkey SG and Johnson GC (2010). Warming of global abyssal and deep Southern Ocean waters between the 1990s and 2000s: Contributions to global heat and sea level rise budgets, *J Clim*, 23, 6336–6351.

Purkey SG and Johnson GC (2012). Global contraction of Antarctic Bottom Water between the 1980s and 2000s, *J Clim*, 25, 5830–5844.

Purkey SG and Johnson GC (2013). Antarctic Bottom Water Warming and Freshening: Contributions to Sea Level Rise, Ocean Freshwater Budgets, and Global Heat Gain. *J Climate*, 26, 6105-6122. doi: 10.1175/JCLI-D-12-00834.1.

Reid JL, Nowlin Jr WD and Patzert WC (1977). On the characteristics and circulation of the southwestern Atlantic Ocean. *J Phys Oceanogr*, 7(1), 62-91.

Reid JL (1989). On the total geostrophic circulation of the South Atlantic Ocean: Flow patterns, tracers and transports. *Prog Oceanogr*, 23, 149– 244.

Rhein M, Stramma L and Send U (1995). The Atlantic Deep Western Boundary Current: water masses and transports near the equator. *J Geophys Res*, 100, 2441-2457.

Rhein M, Stramma L and Krahmann G (1998), The spreading of Antarctic bottom water in the tropical Atlantic, *Deep-Sea Res Part I*, 45, 507– 527.

Rhein M, Kieke D and Steinfeldt R (2015). Advection of North Atlantic Deep Water from the Labrador Sea to the southern hemisphere. *J Geophys Res Oceans*, 120, 2471–2487. doi:10.1002/2014JC010605.

Richardson PL and Fratantoni DM (1999). Float trajectories in the deep western boundary current and deep equatorial jets of the tropical Atlantic. *Deep-Sea Res II*, 46, 305-333.

Robertson R, Visbeck M, Gordon AL and Fahrbach E (2002). Long-term temperature trends in the deep waters of the Weddell Sea. *Deep-Sea Res II*, 49, 4791–4806.

Rühs S, Getzlaff K, Durgadoo JV, Biastoch A and Böning CW (2015). On the suitability of North Brazil Current transport estimates for monitoring basin-scale AMOC changes. *Geophys Res Lett*, 42,8072–8080. doi:10.1002/2015GL065695.

Sandoval FJ and Weatherly GL (2001). Evolution of the deep Western Boundary Current of Antarctic Bottom Water in the Brazil Basin. *J Phys Oceanogr*, 31(6), 1440-1460.

Sarafanov A, Sokov A and Demidov A (2007). Water mass characteristics in the equatorial North Atlantic: A section nominally along 6,5°N, July 2000. *J Geophys Res*, 112, C12023.

Schott FA, Dengler M, Brandt P, Affler K, Fischer J, Bourles B, Gouriou Y, Molinari RL and Rhein M (2003). The zonal currents and transports at 35°W in the tropical Atlantic, *Geophys Res Lett*, 30 (7), 1349.

Schott FA, Dengler M, Zantopp RJ, Stramma L, Fischer J and Brandt P (2005). The shallow and deep western boundary circulation of the South Atlantic at 5°– 11° S. *J Phys Oceanogr*, 35, 2031 – 2053.

Shimada K, Aoki S, Ohshima KI and Rintoul SR (2012). Influence of Ross Sea Bottom Water changes on the warming and freshening of the Antarctic Bottom Water in the Australian-Antarctic Basin. *Ocean Sci*, 8, 419-432.

Sloyan BM and Rintoul SR (2001). The Southern Ocean limb of the global deep overturning circulation. *J Phys Oceanogr*, 31, 143–173.

Spain P, Dorson DL, Rossby HT (1981). Pegasus: A simple acoustically tracked, velocity profiler, *Deep-Sea Res I*, 28A, 1553- 1567.

Speer KG and Zenk W (1993). The flow of Antarctic Bottom Water into the Brazil Basin. *J Phys Oceanogr,* 23, 2667–2682.

Swingedouw D, Fichefet T, Goosse H and Loutre MF (2009). Impact of transient freshwater releases in the Southern Ocean on the AMOC and climate. *Clim Dyn*, 33, 365–381.

Tarakanov, RY (2012). The Scotia Sea and the Drake Passage as an orographic barrier for the Antarctic Circumpolar Current. *Oceanology*, 52 (2): 157-170.

Tarakanov RY and Morozov EG (2015). Flow of Antarctic Bottom Water at the output of the Vema Channel. *Oceanology*, 55(2), 153-161. doi: 10.1134/S0001437015010166

Tsuchiya M, Talley LD & McCartney MS (1994). Water mass distribution in the western South Atlantic: A section from South Georgia Island (54°S) northward across the equator. *J Mar Res*, 52, 55-81.

van Aken HM and de Boer CJ (1995). On a synoptic hydrography of intermediate and deep waters masses in the Iceland basin. *Deep-Sea Res*, 42, 165-189.

Vanicek M and Siedler G (2002). Zonal fluxes in the deep water layers of the western South Atlantic Ocean. *J Phys Oceanogr*, 32(8), 2205-2235.

van Wijk EM and Rintoul SR (2014). Freshening drives contraction of Antarctic Bottom Water in the Australian Antarctic Basin. *Geophys Res Lett*, 41, 1657–1664. doi:10.1002/2013GL058921.

Weiss RF, Bullister JL, Gammon RH and Warner MJ (1985). Atmospheric chlorofluoromethanes in the deep equatorial Atlantic. *Nature,* 314, 608 – 610. doi:10.1038/314608a0.

Wienders N, Arhan M and Mercier H (2000). Circulation at the western boundary of the South and Equatorial Atlantic: exchanges with the ocean interior. *J Mar Res*, 58, 1007-1039.

WOCE Hydrographic Programme Office 1991 WOCE Operations Manual, Section 3.1.2: Requirements for WHP data reporting (Rev. 1), WHPO 90-1. 71pp.

Wüst G (1935). Schichtung und Zirkulation des Atlantischen Ozeans: Die Stratosphäre. In: Wissenschaftliche Ergebnisse, Deutsche Atlantische Expedition auf dem Forschungs – und Vermessungsschiff Meteor 1925–1927. Editor: Albert Defant. *Berlin*: Walter de Gruyter & Co., No. 6 (1). Print.

Yagou H, Ohtake Y, and Belyaev AG (2002). Mesh Smoothing via Mean and Median Filtering Applied to Face Normals. *Proc Geometric Modeling and Processing Conf*, 124-131.

Zangenberg N and Siedler G (1998). Path of the North Atlantic Deep Water in the Brazil Basin. *J Geophys Res*, 103 (C3), 5419-5428.

Zenk W, Siedler G, Lenz B and Hogg NG (1999). Antarctic Bottom Water flow through the Hunter Channel. *J Phys Oceanogr*, 29(11), 2785-2801.

Zenk W and Morozov E (2007). Decadal warming of the coldest Antarctic Bottom Water flow through the Vema Channel, *Geophys Res Lett*, 34, L14607.

Zenk W and Visbeck M (2013). Structure and evolution of the abyssal jet in the Vema Channel of the South Atlantic, *Deep-Sea Res II*, *85*, 244–260.

Zhang D, Msadek R, McPhaden MJ and Delworth T (2011). Multidecadal variability of the North Brazil Current and its connection to the Atlantic meridional overturning circulation. *J Geophys Res*, 116, C04012, doi:10.1029/2010JC006812.

Highlights

- Analysis of hydrographic and current observations (1989-2014) in the western equatorial Atlantic.
- Lower NADW and lighter AABW form an interactive transition layer in the northern Brazil Basin.
- Proof of long-term abyssal warming on isobars in the western tropical Atlantic.
- Warming of densest AABW is mainly caused by descent of isopycnal surfaces and volume loss of dense water masses.
- Changes on isopycnal surfaces show warming in the 1990s and cooling in the 2000s.